Multidisciplinary study of the Tindari Fault (Sicily, Italy) separating ongoing contractional and extensional compartments along the active Africa-Eurasia convergent boundary

G. De Guidi[(1)], G. Lanzafame[(2)], M. Palano[(2)], G. Puglisi[(2)], A. Scaltrito[(2)], L. Scarfi[(2)]

[(1)] Dipartimento di Scienze Geologiche, Università di Catania, Catania, Italy.

[(2)] Istituto Nazionale di Geofisica e Vulcanologia, Osservatorio Etneo - Sezione di Catania, Catania, Italy

Abstract

The Africa-Eurasia convergence in Sicily and southern Calabria is currently expressed by two different tectonic and geodynamic domains: the western region, governed by a roughly N-S compression generated by a continental collision; the eastern one, controlled by a NW-SE extension related to the south-east-directed expansion of the Calabro-Peloritan Arc. The different deformation pattern of these two domains is accommodated by a right-lateral shear zone (*Aeolian-Tindari-Letojanni fault system*) which, from the Ionian Sea, north of Mt. Etna, extends across the Peloritani chain to the Aeolian Islands.

In this work, we study the evidence of active tectonics characterizing this shear zone, through the analysis of seismic and geodetic data acquired by the INGV networks in the last 15 years. The study is completed by structural and morphological surveys carried out between Capo Tindari and the watershed of the chain. The results allowed defining a clear structural picture depicting the tectonic interferences between the two different geodynamic domains. The results indicate that, besides the regional ~N130°E horizontal extensional stress field, another one, NE-SW-oriented, is active in the investigated area. Both tension axes are mutually independent and have been active up to the present at different times. The coexistence of these different active horizontal extensions is the result of complex interactions between several induced stresses: 1) the regional extension (NW-SE) related to the slab rollback and back-arc extension; 2) the strong uplift of the chain; 3) the accommodation between compressional and extensional tectonic regimes along the Aeolian-Tindari-Letojanni faults, through a SSE-NNW right-lateral transtensional displacement. In these conditions, the greater and recurring uplift activity is not able to induce a radial extensional dynamics, but, under the "directing" action of the shear system, it can only act on the regional extension (NW-SE) and produce the second system of extension (NE-SW).

Key words: Africa-Eurasia convergence; Aeolian-Tindari fault system; transform activity; stress and strain fields; multidisciplinary approach.

1.0 Introduction

The present-day tectonic framework of Sicily is the result of the Neogene-Quaternary geodynamic processes related to the *ca*. N-S Africa and Eurasia convergence (e.g. Barberi et al., 1973; Patacca et al., 1990) leading to the building of the Apennine-Maghrebian chain. To date, the Africa-Eurasia interaction is expressed by continental collision in western Sicily and by the subduction and rollback of the Ionian oceanic crust underneath the Calabro-Peloritan Arc (CPA) and the Tyrrhenian Sea (Malinverno and Ryan, 1986; Faccenna et al., 2001). Within this complex geodynamic framework, both a compressional and an extensional tectonic domain can be recognized (Bousquet et al., 1988; see Fig. 1). The former controls western and central Sicily and the southern Tyrrhenian off-shore through the action of WNW-ESE to N-S compressive axes (Bousquet and Lanzafame, 1995; Caccamo et al., 1996; Monaco et al, 1996; Montone et al., 2004; Neri et al., 2005; Billi et al., 2007; Palano et al., 2012). On this larger compressive western domain, an incipient extension lying between Cefalù and Mt. Etna can be recognized, which is believed to derive from upper crustal stretching above an active thrust belt (Lavecchia et al., 2007) or as the reactivation of pre-existing faults and upwelling of melt mantle material beneath Mt. Etna (Billi et al., 2010). The eastern extensional tectonic domain can be recognized in southern Calabria and north-eastern Sicily, where tectonic and seismological studies (Ghisetti, 1979; Tortorici et al., 1995; Neri et al., 2005; Ferranti et al., 2008; Scarfì et al., 2009) show an extension oriented about N130°E, perpendicular to CPA and parallel to the direction of the subduction. This last is well represented under the Calabria and south-eastern Tyrrhenian region by shallower and deeper seismicity, with foci located down to a depth of about 500 km.

Several models have been proposed to explain the complex geodynamic setting of the central Mediterranean region (e.g. Wortel and Spackman 2000; D'Agostino, 2004; Goes, 2004; Faccenna, 2011 and references therein). However, none of these interpretations coherently reconciles the geological, geophysical, volcanological and neotectonic regional data better than the hypothesis that takes the Ionian subduction beneath the CPA into account, even considering it

almost ended or terminating its evolution passively (Bousquet, 1977; Malinverno and Ryan, 1986).

The Africa-Eurasia collision is diachronic to the east and, from the lower Pliocene, the contemporaneous and adjacent compressional-extensional domains were accommodated by bundles of faults that form a series of right-lateral shear zones (Finetti et al., 1996; Billi et al., 2011) which, over time, have migrated eastward. To date, the easternmost and youngest of these tectonic junctions develops along a NNW-SSE striking fault belt between the Aeolian Islands and the Ionian Sea (*Aeolian-Tindari-Letojanni fault system*, hereinafter ATL; Fig. 1), which appears to be the northward continuation of the Hyblean-Maltese fault system (e.g. Cristofolini et al., 1977; Ghisetti, 1979; Govers and Wortel, 2005 and references therein), belonging to a diffuse transtensional fault system developed from eastern Sicily up to the north African margin (Corti et al., 2006). This possibility was already suggested by Vecchia (1963) based on the distribution of the gravimetric anomalies. Lanzafame and Bousquet (1997) attribute to this system, 350-400 km long, a transform role with respect to the Aeolian volcanic arc. The complex structural picture of this region is further convoluted by strong tectonic uplifting induced by the isostatic response of a long and hard thrusting history, which led to the formation of a mountain belt and the doubling of the crust beneath the Tyrrhenian side of the chain. The final uprising started after the deposition, in basins some hundreds of meters deep, of middle Pleistocene (600-500 kyr) clay sediments, which today are uplifted to an elevation up to 560 m a.s.l. The cumulative tectonic vertical movement (*ca*. 1000 m in 0.5 Myr) currently represents an important component making up and controlling the dynamics of the region (Catalano et al., 2008).

In recent years, significant seismic activity has characterized the area along the Tyrrhenian on-shore segment of the ATL, particularly close to the Tripi village (see Fig. 2), with frequent, sometimes daily (e.g. January 2011), earthquakes (for details see http://www.ct.ingv.it/ufs/analisti/list.php). This seismicity, still ongoing, has stimulated our interest and in this work, we study the transitional area between ongoing contractional and extensional crustal compartments, focusing on the zone between Capo Tindari, Tripi and the top of the Sicilian

chain. Therefore, starting from the noteworthy scientific results related to the same area (e.g. Billi et al., 2006; 2010), we applied a multidisciplinary approach to include tectonic, morphological, seismological, geodetic and archaeological data, looking for clear evidence of recent to historical motions on the fault system. In this way, we were able to obtain a detailed spatial resolution of the horizontal strain-rate and stress fields and to deepen our knowledge of this active sector and of the main tectonic processes and their evolution.

2.0 Geological Setting

The ATL is a regional belt of brittle deformation located in north-eastern Sicily, extending from the Ionian Sea, north of Mt. Etna, to the Aeolian Islands, at the release between the ongoing compressional and extensional crustal domains related to the Africa-Eurasia convergence process. This fault system has probably formed as a consequence of the Middle Pleistocene tectonic reorganization in the south-central Mediterranean, characterized by the slowing or cessation of Calabrian roll-back and subduction, and back-arc Tyrrhenian extension (Westaway, 1993; Wortel and Spakman, 2000; Goes et al., 2004; Palano et al., 2012). Today, it cuts the south Tyrrhenian Sea and the Peloritan chain (part of the Apennine-Maghrebian chain) and consists of a NNW striking set of normal faults, characterized by steeply inclined scarps (dip $\geq 60°$) that mostly dip eastward and having both a predominantly dip-slip kinematics and, subordinately, a significant right-lateral one (Atzori et al., 1978; Ghisetti, 1979). Near the Tyrrhenian coast, a part of the main ATL is known as Tindari fault line (hereinafter TFL), which has a very impressive morphological expression for 20 km in length, between Capo Tindari, Tripi and Rocca Novara at the top of the chain (Fig. 2). Along the coast, Ghisetti (1979) indicates that, across the TFL, the Tyrrhenian terraces reveal a vertical offset of about 50-60 m and the Plio-Quaternary terrains show right-lateral movements of about 6-7 km. However, very little is known about the temporal relationship between these movements and their spatial distribution along the whole ATL. Published age constraints only allow dating the fault activity in this area to as recent as the middle-upper Pleistocene (Ghisetti, 1979; Catalano and Di

Stefano, 1997). Nevertheless, the fault system is seismically active especially along its off-shore segment until the Aeolian Islands (Neri et al., 2005; Scarfì et al., 2005; Langer et al., 2007) and, on-shore, in the Tripi zone until Novara di Sicilia (Giammanco et al., 2008). To the south, across the chain, morphological expressions of the ATL are less evident, since the terrains traversed (Hercynian metamorphic basement) make it more difficult to keep track of faulting activity. Consequently, the southern termination of the fault system has been widely debated, but several authors extend the southern tip of the fault to the Ionian coast of Sicily (e.g. Govers and Wortel, 2005; Palano et al., 2012) and eventually link the fault system with the Hyblean-Maltese fault system (e.g. Lanzafame and Bousquet, 1997).

On the north side of the Peloritani chain, the TFL is completed also by second-order N-S- and NE-SW-striking extensional faults (Fig. 2), with dip-slip and left oblique kinematics. Parallel to the coast, on- and off-shore, there are both E-W- and ENE-WSW-striking fault systems; these faults, having N-dipping steeply inclined scarps (dip $\geq$ 70°), are indicated as being largely responsible for the uplift of the region (Lentini et al., 2000). The complex configuration of these fault systems form a triangular tectonic depression whose vertices are Rocca Novara, Capo Tindari and Barcellona P.d.G. (Fig. 2). In this area, the Hercynian metamorphic basement of the chain outcrops extensively and is covered by an allochthonous sedimentary succession made up of: 1) the Stilo-Capo d'Orlando flysch (Late Oligocene-Early Burdigalian; Bonardi et al., 1980; Cavazza et al., 1997; Lentini et al., 2000), 2) a Cretaceous clay-rich mélange (Varicolori Clays), attributed either to back-thrusting (Ogniben, 1960) or to re-sedimentation (Cavazza et al., 1997), and 3) biogenic sandstones with calcareous cement (Langhian; Floresta calcarenites, Auct). On the coastal zone, this thrust-edifice is covered by a discontinuous marine and continental sequence of Pliocene-Holocene deposits (clay, marls, sandy-clays, sand and conglomerates; Lentini et al., 2000).

3.0 Methods, Data and Results

In the following paragraphs, we illustrate in detail the analyses carried out on geodetic,

seismological and geological data and the related results.

3.1 Geodesy

GPS monitoring of the ground deformations of Peloritani-Nebrodi area started in late 1995, when a geodetic network was set up by the Istituto Internazionale di Vulcanologia, merged into the Istituto Nazionale di Geofisica e Vulcanologia in 2001; Fig. 1c (Puglisi et al., 1999). The network consisted of 7 self-centring benchmarks and has successively been expanded to reach the current configuration of 12 benchmarks. The overall network, surveyed in 1996, 1998, 2002, 2003 and 2006, was previously analyzed in Mattia et al. (2009). Because some benchmarks are shared with the Mt. Etna network reference frame (Palano et al., 2010 and references therein), which is measured annually, we re-analysed all GPS data, in order to improve the ground deformation pattern over the investigated area.

GPS data were processed by using the GAMIT/GLOBK software (Herring et al., 2010) according to the strategy described in Palano et al. (2011). To improve the overall configuration of the network and to tie the regional measurements to an external global reference frame, data acquired by 10 continuously operating IGS stations (AJAC, CAGL, GRAS, GRAZ, LAMP, MATE, MEDI, NOT1 and NOTO) were included in the processing.

The geodetic velocity field, rotated in a fixed Eurasian frame (Mattia et al., 2008) and reported in Fig. 3a, is characterized by a general N-directed motion with a fan-shaped feature according to a previously published velocity field (Mattia et al., 2009). In particular, going from west toward east, the velocity field is characterized by a rotation from an azimuth of ~N15°W to an azimuth of ~N15°E, evidencing a diverging pattern between the sites located across the TFL. By applying a vector decomposition of the velocities of stations located across the TFL (CALA, TIND and MONT on the left and NOVA and RODI on the right), we estimated the rates of parallel (i.e. strike-slip) and perpendicular (i.e. tensile or opening) movement. Using a mean N35°W fault trend, through a Monte Carlo resampling, we estimated a tensile and a strike-slip component of 1.1 ± 0.5 and -3.4 ± 0.7 mm/yr (negative for dextral shear), respectively.

To investigate the strain field across the TFL, we divided the region into quadrilaterals (with vertices defined by GPS sites; labelled as P1, P2, P3, P4, P5 and P6 on Fig. 3b). By using the formulation of Allmendiger et al. (2007), we estimated the 2D strain-rate components at the center of each quadrilateral (see Supplementary materials for details). The main results are reported in Fig. 3b as greatest extensional (ε_{Hmax}) and contractional (ε_{hmin}) strain-rates. Westward of the TFL, on P1, the strain-rate pattern is poorly quantified since it is very close in magnitude to the associated uncertainties, while on P2, it clearly depicts a prevailing NNE-SSW extension (*ca*. 430 nanostrain/yr) coupled with a small shortening component (*ca*. 50 nanostrain/yr); across the TFL the strain-rate field shows a prevailing NW-SE extension (*ca*. 320 nanostrain/yr) on P3, matching well the results previously found by the vector decomposition of the velocities of sites located across the TFL (in this study) and the results achieved in Mattia et al. (2009). P4 is characterized by a prevailing N-S-oriented extension (*ca*. 115 nanostrain/yr). Eastward of TFL, the strain rates pattern is sampled by P5 and P6: the former is characterized by a prevailing NW-SE extension (*ca*. 220 nanostrain/yr) while the latter shows a prevailing N-S-oriented extension (*ca*. 160 nanostrain/yr). Roughly speaking, the observed strain rate pattern clearly highlights how the investigated area is characterized by a general crustal stretching.

3.2 Seismicity

We analyzed the seismicity occurring in north-eastern Sicily from 1999 to 2010 by using the data recorded by the local network operated in eastern Sicily, southern Calabria and Aeolian Islands, firstly by the "Poseidon Project" then merged into the Istituto Nazionale di Geofisica e Vulcanologia in 2001 (Fig. 1c). In the investigated area, more than 1000 earthquakes with magnitude ranging from 1.0 to 4.2 were located (Fig. 4a). By observing the hypocenter distribution, we recognize a concentration of foci in the eastern part of the studied area, between the town of Castroreale and the Gulf of Patti (Fig. 4b). Many of these earthquakes occurred as swarms (Fig. 4a) and often as multiplets. The pattern of this seismicity was studied in detail by Scarfì et al. (2005)

and Giammanco et al. (2008), who claim evidence for fluid interaction and involvement with normal faults in the triggering mechanism of these earthquakes at middle crustal depth (8-15 km). In particular, the dense network of tectonic structures in the area could provide potential drainage pathways for any fluid overpressures that may develop at depth. Westward, from Capo Calavà, a NW-SE oriented alignment of earthquakes is visible. Finally, very few events occurred in the western part of the studied area, but this factor must be read with caution as the ability to detect small earthquakes diminishes due to the unfavourable network configuration. The depth of the foci is typically between 7 and 15 km. The cluster located south-east of Capo Calavà shows greater focal depth (18-25 km).

The use of a dense seismic network allowed computing and constraining focal plane solutions (FPSs) well for earthquakes with local magnitudes (M_L) less than 3.0. To this end, we carefully selected events from the basic dataset, considering only those with at least ten first motion P-polarities (typically, events with $M_L \geq 2.5$), with sufficient station coverage on the focal sphere. As a result, we were able to calculate focal mechanisms for 69 earthquakes (Table 1), with 15 impulsive P-wave first motions on average. The events were relocated with the minimum 1D velocity model by Langer et al. (2007) and the nodal planes were identified using the code of Reasenberg and Oppenheimer (1985).

Analyzing the results, we can identify two areas where the FPSs are fairly homogeneous. In particular, for the earthquakes located in the Castroreale area and along the coast of the Gulf of Patti, the FPSs show normal faulting features with NE-SW-striking nodal planes and NW-SE-striking T axes (Fig. 5a). Off-shore from the Gulf of Patti, earthquakes show a prevailing strike-slip faulting mechanism, with T-axes oriented NW-SE. For the other areas, we found mainly normal fault solutions, with T axes striking NW-SE as well as NE-SW. Only four reverse faults with NW-SE oriented rupture planes were observed; two just south of Capo Calavà at a depth of 17 and 27 km and two in the western sector at a depth of 6 and 12 km.

Then, we applied the Gephart and Forsyth (1984) procedure to invert the focal mechanisms

to determine the principal stress axes (σ_1, σ_2, σ_3) and the dimensionless parameter $R=(\sigma_2-\sigma_1)/(\sigma_3-\sigma_1)$ that describes the relative magnitudes of the principal stresses. The method identifies the best stress tensor model that most closely matches all the fault plane solutions of the source region. It requires the basic assumption that the stress is uniform in space and time domains in the investigated volume. A misfit variable (F), given by the angular difference between the observed slip direction on a fault plane and the shear stress derived from the stress model, provides a guide to how well the assumption of stress homogeneity is fulfilled (Michael, 1987).

First, we performed an inversion with the whole focal mechanism dataset. The result indicates a stress tensor with a near-horizontal σ_3 (plunge 4°) and σ_2 (plunge 28°) (see Fig. 5). The 95% confidence intervals of the principal stress axes do not overlap, indicating that the three axes are well-constrained by the data (Gephart and Forsyth, 1984; Parker and McNutt, 1980). However, the minimum average misfit of 7.6° suggests that the solution may reflect some heterogeneity (Wyss et al., 1992). Indeed, grouping small-magnitude earthquakes over a large area may produce misleading results, due to possible lateral variations of the stress orientations (and stress ratio). This might be complicated by the fact that small-magnitude earthquakes could be characterized by internal kinematic complexities, even under a homogeneous regional stress field (e.g. Carey-Gailhardis and Mercier, 1992). In order to avoid these problems as much as possible and considering also the main objectives of this study, we performed further inversions by grouping FPSs in four small areas (Fig. 5a) taking account of their (1) kinematics, (2) focal depths and (3) epicentral distribution with respect to TFL. Considering each resulting reduced stress tensor, we computed the Sh_{min} orientation by adopting the formula given by Lund and Townend (2007).

The main results are reported in Fig. 5b. A1 area, located in the southern Tyrrhenian (Gulf of Patti), is characterized by a near-horizontal σ_3 (plunge 26°) and σ_1 (plunge 14°), evidencing a strike-slip stress regime with a Sh_{min} N102°E oriented. Southward, on the eastern side of TFL, on- and off-shore of the coastal zone, A2 area is characterized by a sub-vertical σ_1 (plunge 82°), evidencing a normal faulting stress regime with a Sh_{min} N130°E oriented. South-westward, on the

chain across the TFL, A3 area is characterized by a sub-vertical σ_1 (plunge 60°), evidencing a normal faulting stress regime with a Sh_{min} N11°E oriented, orthogonally oriented with respect to the one inferred for A2 area. In addition, A3 area is also characterized by a stress ratio R of 0.65 denoting that σ_2 is rather close in its absolute value to σ_3, containing focal mechanisms similar to those observed in the A2 dataset. The A4 area, located about 30 km west of TFL, grouped only six FPSs with different kinematics, making it very difficult to constrain the stress tensor; for this reason, we excluded this area from our analysis.

3.3 Geology and Neotectonics

A detailed field survey and structure mapping was carried out in the triangular tectonic depression and along its western and eastern boundaries (Fig. 2), in order to collect geomorphologic and neotectonic faulting data, for the Holocene period. We thus marked the more recent deformations using archeological dating and the morphological features that are inscribed on the last rejuvenation of landscape. In the field, we studied the geometry and kinematics of fault surfaces and relative striations at 7 different measurement sites, collecting more than 40 slip data. These data were used for quantitative determination (numerical method) of the principal stress orientation (Table 2), while observations on large faults allowed obtaining qualitative determinations through classic graphical methods. In the following, we describe our findings for each measurement site in detail (Fig. 2).

In the north-western sector of the studied area, 3.8 km south of Capo Tindari, close to the coast, the present-day coastal-fluvial plain is cut by a well-exposed N15-30°E-striking, 60°-eastward dipping extensional fault (site 1 in Fig. 2 and Fig. 6), characterized by clear double sets of striations with dip-slip striae (pitch 70°N; ENE-WSW extension) overprinting the right-lateral ones (pitch 30°S; NNW-SSE extension). Southward, immediately to the west of the Tripi cemetery (site 2 in Fig. 2), the TFL exhibits a spectacular fault scarp (Fig. 7a). This segment has a N140°E attitude, and a 70°-eastward dip; it normally dissects the range, forming a 250 m high triangular

facet and evidencing rapid footwall uplift. Since stratigraphic references across the fault are lacking, we cannot measure the cumulative throw. However, considering that erosion has removed the entire sedimentary succession, exposing the metamorphic basement in the rising footwall, we can assume a vertical throw of more than 1000 m. This large throw results from a long polyphasic activity as testified by the occurrence of a roughly 2 m wide cataclastic band (Fig. 7b), coating the motion plane, and by a well-developed Holocenic piedmont talus at the base of the fault escarpment (Fig. 7c). The cataclastics, the bedrock and the surfaces of some elements making up the talus, show many striated planes (stereographic projection in Fig. 7a), indicating repeated faulting events and superimposition of different displacements, with prevalent dip-slip associated with right-lateral ones (e.g. extensions along N40°E and N125°E; Fig. 2 and Table 2). Further south, within the floodplain of "Torrente" (small river) Mazzarrà (Fig. 8a), the morphological evidences of the fault line are lacking for 4 km, but the effects of its activity can easily be recognized: just south of the cut talus (Fig. 7c), at the confluence of Mazzarrà and Tripi streams, the alluvial fan of the latter river cannot be related to any hydraulic processes but, according to the scheme of river response to tectonic deformation (Holbrook and Schumm, 1999), it is clearly linked to the current fault activity for which we can determine, through topographic measurements, vertical uplift in historical time. Indeed, in the rising footwall, the fluvial erosion cuts the Tripi river fan, exposing remnants of late-Roman terracotta (1500 yr before present; Figs 8b,c), uplifted less than 3 m with respect to the floodplain of Mazzarrà river (downthrown). On this downthrown eastern side of the fault, some water wells, older than 70 yr, are stable and have not been eroded or flooded (Fig. 8d). These observations are in agreement with the longer time and a regional scale functioning of the faults (Lentini et al., 2000), as noted for example at Barcellona P.d.G., where Middle-Pleistocene clays outcrop at 75 m a.s.l. within the tectonic depression, while they are uplifted to 563 m a.s.l. on the neighbouring footwalls: the dip-slips of the dislocations are mainly due to the uplift of the footwall, and are the major components of the regional uplift.

Even further south, the morphological evidences of the TFL can be recognized once again at

Rocca Novara (site 3 in Fig. 2) which, under the evident control of the line faults, is structured to form a prominent horst (Fig. 9a), extending for about 3 km along the NNW-SSE direction. Many elements testify to the young tectonic activity of these faults: 1) the fresh morphologic features of the horst; 2) the well-preserved triangular facets in the degradable phyllite rocks; 3) the most eastern fault of the horst that, at Serro Rosano, vertically displaces the Holocenic rock flow by about 40÷50 m (α and α' in Fig. 9a); 4) the free face at the base of the fault escarpment (NW-SE, 70°NE; Fig. 9b), at the northeastern end of the horst (M. Santa Croce; site 4 in Fig. 2). Numerical analysis (Fig. 9c and Table 2) shows that the kinematics of this part of the TFL is normal (N60°E extension), accompanied by less evident right-lateral extensional slips (N130°E extension).

The eastern side of the triangular depression consists of main faults, prevailingly N-S and NE-SW oriented, with steeply inclined scarps (dip ≥ 60°) generally westward dipping, characterized by extensional dip-slip and left-lateral strike-slip kinematics. In this context, there are also faults in line with the TFL, and a clear example of a very young oblique movement has been detected on the right side of the Brandino river (site 5 in Fig. 2) where a N120-130°E-trending fault, 40-50°SW dipping, displaces the Holocenic piedmont deposits (Fig. 10a) with left-normal kinematics (pitch 30°SW; NNW-SSE extension). Southward, on the opposite side of the Brandino river (site 6 in Fig. 2), a N10°E normal fault, dip 45°W, pitch 65°S, displaces the present-day vegetated soil and the low grade metamorphic bedrock by about 1 m (Fig. 10b), indicating an active ENE-WSW extension. Further south, just above the Giarra village (site 7 in Fig. 2), a large normal fault (Fig. 11), N40°E-trending, 65-70°SE dipping, with an offset of about 30-40 m following an almost vertical trajectory (pitch 65-70° SW), is recognized. The discontinuity cuts the active range front and displaces a narrow V-valley which, in the raised footwall block, remains hanging between two faceted ridges: despite the Palaeozoic age of the dissected rocks, this prominent and fresh morpho-structural organization shows the young Holocenic activity of the fault under an ~NW-SE extension.

To summarize, the structural framework of the studied area is strongly controlled by

impressive normal fault planes with dominant dip-slip movements; however these kinematics are usually accompanied by striations originating from lateral motions. More generally, the main features inferred by our study are: 1) all the faults are extensional; 2) the faults are arranged in two main systems ca. NNW-SSE- and NE-SW-oriented; 3) the geometry and the kinematics of the faults cannot be considered as a conjugate system, therefore they are not compatible with a unique stress field but, on the contrary, the faults move under two different directions of horizontal extension. Both can be represented by two stress ellipsoids that maintain similar orientations and have always a vertically σ_1, whereas σ_2 e σ_3 are horizontal, roughly NE-SW and NW-SE oriented (from NNE-SSW to NE-SW and from NNW-SSE to NW-SE), and can change mutually; 4) both the extension directions act independently and are still currently active; 5) the faults (often the same planes) can act with dip-slip, strike-slip, or oblique kinematics, according to the heavy fracture state of the rocks, and the geometric combination between fault planes and stress orientations; 6) the structural and morphological overview of this area is controlled by the impressive uplift of the chain, that essentially comes about through the dip-slip faults and that draws vertical striations on almost every dislocation plane; 7) the fault displacements reached a cumulative vertical movement higher than 1000 m (Tripi) and were active in very recent times (Giarra, Serro Rosano; slip-rate up to 3-4 mm/yr) up to the historical period (1500 yr before present at Tripi river; 2 mm/yr). Keeping in mind that in the area, most of the regional uplift (in Barcellona P.d.G., around 90%) occurs through the dip-slip faults (Lentini et al., 2000), we inferred that the uplift rates of the chain axial is greater than those estimated for the coastal areas (1-1.5 mm/yr; Stewart et al., 1997; Catalano et al., 2003; 2008).

4.0 Discussion and Conclusions

The kinematic setting of TFL was studied through a multidisciplinary approach, including geodetic, seismological, tectonic, morphological, and archaeological data. In particular, we investigated the strain-rate field measured geodetically and the tectonic stress pattern as estimated

by using focal mechanisms (at depth) and fault slip (on the surface) data.

Both strain-rate and stress fields are reported in Fig. 12. Since the investigated area shows prevailing extensional tectonic features, we chose to show both the direction of the minimum compressive horizontal stress (Sh_{min}) and the maximum extensional strain-rates (ε_{Hmax}). The simple visual comparison allows inferring that eastward of TFL both Sh_{min} and ε_{Hmax} are aligned along the NNW-SSE trend, while westward of TFL, they are aligned along the NNE-SSW direction. On the TFL, geological data highlights how both the two extensional directions coexist.

Furthermore, it is important to note that we compared stresses at depth (close to the surface for fault slip data and from 5 km to 20 km for earthquake focal mechanisms) with strain-rates observed at the surface; hence, we may expect some differences if there is a depth dependence of the processes causing the stress and strain-rate fields. However, we observed an excellent agreement between the Sh_{min} and the ε_{Hmax} directions, indicating that both the deep and shallow crust in the investigated area is extending in the direction of least compression. This indicates that the deformation processes causing the earthquakes and the geodetically determined surface deformation are driven by the same forces.

Along the TFL these stress fields can be described by different 3D axis orientation but with the direction of their principal axes unchanged. In particular, the ellipsoids are usually characterized by a vertical σ_1, while σ_2 e σ_3 can mutually change on the horizontal plane, with roughly NE-SW and NW-SE directions. The two extensional axes are almost perpendicular and independent and have been active at different times to date. The seismological data indicate that the contemporaneous activity of the two extensional axes becomes more significant (Fig. 5) on moving from the coastal areas to the axial zone of the chain (A3 in Fig. 5a). Evidently, the thicker and heavier the thrust-edifice, the greater the isostatic push, suggesting the uplift of the chain as one of the main factors in making up the fabric of the tectonic stresses dominating the entire region. In this framework, most of the general lifting is achieved by the vertical activities on the faults (Lentini et al., 2000). Therefore, the hypothesis that the axial zone of the chain is affected by a greater uplift

with respect to the peripheral areas (1-1.5 mm/yr; Stewart et al., 1997; Catalano et al., 2003; 2008), fits with the rate of the fault dip-slips that may be ascribed to historical (2 mm/yr; Tripi river) and Holocenic (3-4 mm/yr, Serro Rosano and Giarra) times, compared with uplift rates measured, for the heart of the Apennine edifice, in Taormina (2.1 mm/yr; Stewart et al., 1997) and in the Messina Straits (1.8-2.1 mm/yr; De Guidi et al., 2003; Ferranti et al., 2007).

Therefore, the unusual structural pattern of this sector of the chain, does not easily fit a deformative model that only takes the ~N130°E regional extension into account. Similarly, we cannot invoke the stresses linked to the chain uplift alone to explain the contemporaneous activity of the two independent extensions. Indeed, the uplift should induce radial extension, cylindrically distributed, and the dispersion of the σ_3 on the horizontal plane as described by a two axes ellipsoid ($\sigma_2 = \sigma_3$). Our data can instead be easily integrated in a coherent regional deformation pattern that combines the uplift, the regional extension and the activity of the TFL which, on a regional scale, accommodates the western compression and the eastern distension. Within this peculiar and complex composition, we followed the idea of Hancock et al. (1987), who found consistent applicability to both outcrops and the regional scale (Caputo, 1995; 2010), as well as the Aeolian active volcanic arc (Falsaperla et al., 1999). This scheme suggests that the stress field, resulting from the ~N130°E regional extension (σ_1 vertical, σ_2 e σ_3 horizontal and with almost similar magnitude), may be contrasted by the frequent phases of strong uplift that reduce the σ_1 (the weight of the chain). This in turn triggers the stress swap between σ_2 and σ_3, up to generating a second system of active extension (ca. NE-SW), which temporally dominates the entire region, controls its morphological and tectonic evolution and continues to rejuvenate the fault planes. In this deformative process, the interaction between the extensional regional stresses and the ones induced by the uplift, prevent the horizontal dispersion of the tension axes during the stronger phases of uplift. The ATL probably also acts with the same effect, which has a leading action on the azimuthal arrangement of the stress field because it is a first order crustal discontinuity. Under the ~N130°E regional extensional stress field, the NE-SW-oriented fault planes act with dip-slip

kinematics, the TFL acts with right lateral displacements and the NNE-SSW-oriented faults act with left lateral motions. Such deformation events are rare in comparison with the most frequent uplift inputs and this accounts for the striated fault planes in which the frequent dip-slip movements usually overprint the striations related to the regional ~N130°E extension.

Concerning the general uplift of the chain (Catalano and Di Stefano, 1997), our results confirm that this process has also been active after the Roman age and takes place mainly through the vertical activity of the faults, where the regional isostasy has little influence. In contrast with Lentini et al. (2000), not only the Apenninic faults, but also the discontinuities belonging to TFL and other structural systems crossing the chain, with vertical cumulative throw greater than 1000 m (Tripi), played a role in the rise of the chain.

Within the current geodynamic context, the ATL is interpreted by most investigators as a diffuse transtensional boundary between the adjacent contractional and extensional crustal domains (Carminati et al., 1998, Govers and Wortel, 2005; Argnani et al., 2007). By modelling the ground deformation pattern, Mattia et al. (2009) pointed out that some discrete segments of ATL are active. Moreover, earthquakes and neotectonic data analyzed in this study reveal that the ATL is still seismically active, especially along its off-shore segment until the Aeolian Islands and on-shore (where the fault system is termed as TFL), until the Novara di Sicilia area. Southwards, across the chain, morphological evidence of ATL is lacking and there are no clear traces of neotectonic activity of this fault system. However, based on the analyses of additional geodetic data, Palano et al. (2012) evidenced that the southward extension until the Ionian coast of the ATL is feasible. This aspect suggests that even if no clear traces of neotectonic activity of the fault system can be recognized in the area comprised between Novara di Sicilia and the Ionian coast, the deformation could be partitioned into a diffuse network of short fault segments (with length ranging in between 0.5 - 5 km) and transferred from the chain up to the Ionian coast. In this picture, the crustal thickness (CT) beneath the investigated area could play a crucial rule in the development and activity of this fault system: between the Aeolian Islands (CT ~ 18 km) and the northern Sicilian

coastal area (CT ~ 25 km) the ATL is seismically ongoing and tectonically active. Southwards across the chain, the thicker chain (CT > 30 km) and the coupled crust beneath the orogen offer a higher mechanical strength to the formation of a well-developed shear zone: here the fault system is developed as a diffuse network of short fault segments without significant seismicity. Taking all these aspects into account, if such a fault system is developing across the chain, it should be in its inception stage.

Another important question is related to the possible offshore extension of the ATL fault system and its relationship with the Ionian accretionary prism. The presence in the Ionian basin of NNW-SSE to NW-SE trending structures (Nicolich et al., 2000; Argnani and Bonazzi, 2005; Polonia et al., 2011), to which several earthquakes with prevailing strike-slip focal mechanisms can be associated (Scarfì et al., 2009), suggests that the possible offshore extension of ATL is feasible. More problematic is to understand if ATL is linked to the seismically active Hyblean-Maltese fault system offshore of eastern Sicily (Lanzafame and Bousquet, 1997; Doglioni et al., 2001) or whether it simply connects the north Sicilian contractional belt to the Ionian accretionary prism, accommodating differential movements within the contractional belt (Goes et al., 2004; Jenny et al., 2006; Billi et al., 2006). Despite the lack of clear data, in both scenarios the ATL can be considered as the surface expression of a lateral slab tear (or STEP fault, as defined in Govers and Wortel, 2005), separating the ongoing subduction-rollback processes of the Ionian oceanic to the east from the still active continental collision to the west.

The main results presented and discussed in this study can therefore be summarized as follows:

1) Over the investigated area, we identified two different directions of extension, NW-SE- and NE-SW-oriented, mutually independent and active to date;

2) fault plane solutions indicate that the NW-SE (~N130°E) extension is widespread over the entire investigated area, while the NE-SW extension is sparse in the southern Tyrrhenian Sea and becomes progressively more evident moving from the coastal areas toward the axial zones of

the chain;

3) the regional uplift rate is about 1/1.5 mm/yr close to the coastal area and increases on the axial zones of the chain, where the faults reach a rate of vertical throw up to 3-4 mm/yr;

4) the overall features reported in this work highlight that the regional uplift, coupled with the ~N130°E extension (likely related to the subduction-rollback processes of the Ionian oceanic slab), are responsible for the complex stress field acting on the region;

5) GPS data highlight a right lateral displacement of about 3.4 mm/yr across the TFL.

In conclusion, our findings would indicate that the fault strip of the TFL and of the entire ATL, taken together, produces an active shear zone which takes on a *transform role*, allowing the CPA to continue its southward expansion above the Ionian oceanic crust, while western Sicily remains locked in a continental collision regime. In this interpretation, the activity of the TFL is the response to different deformation regimes occurring in the adjacent compartments, rather than the direct result of the Africa-Europe convergence, and with a NNW-SSE geometry likely inherited from the oldest (Scandone et al., 1981) Hyblean-Maltese escarpment fault system. Nonetheless, the dynamics of the TFL and of the entire region cannot be fully understood unless one considers the stress field linked to the chain uplift, producing the second system of extension (NE-SW).

Acknowledgments

We wish to thank the Editor, Prof. F. Storti, A. Billi and an anonymous reviewer for carefully reading the manuscript and providing constructive criticism. We also thank S. Conway for correcting and improving the English language of this manuscript.

References

Allmendinger, R. W., Reilinger, R., Loveless, J., 2007. Strain and rotation rate from GPS in Tibet, Anatolia, and the Altiplano.Tectonics 26, TC3013, doi:10.1029/2006TC002030.

Argnani, A., Serpelloni, E., Bonazzi, C., 2007. Pattern of deformation around the central Aeolian islands: evidence from multichannel seismic and GPS data. Terra Nova 19, 317-323, doi: 10.1111/j.1365-3121.2007.00753.x.

Argnani, A., and Bonazzi, C., 2005. Malta Escarpment fault zone offshore eastern Sicily: Pliocene-Quaternary tectonic evolution based on new multichannel seismic data. Tectonics 24, TC4009, doi:10.1029/2004TC001656.

Atzori, P., Ghisetti, F., Pezzino, A., Vezzani, L., 1978. Strutture ed evoluzione geodinamica recente dell'area peloritana (Sicilia nord-orientale). Boll. Soc. Geol. Ital., 97, 31-56.

Barberi, F., Gasparini, P., Innocenti, F., Villari, L., 1973. Volcanism of the Southern Tyrrhenian Sea and its geodynamic implications. J. Geophys. Res. 78, 5221-5232, doi: 10.1029/JB078i023p05221.

Billi, A., Barberi, G., Faccenna, C., Neri, G., Pepe, F., Sulli, A., 2006. Tectonics and seismicity of the Tindari Fault System, southern Italy: crustal deformations at the transition between ongoing contractional and extensional domains located above the edge of a subducting slab. Tectonics 25, TC2006, doi: 10.1029/2004TC001763.

Billi, A., Presti, D., Faccenna, C., Neri, G., Orecchio, B., 2007. Seismotectonics of the Nubia plate compressive margin in the south Tyrrhenian region, Italy: Clues for subduction inception. J. Geophys. Res. 112, B08302, doi:10.1029/2006JB004837.

Billi, A., Presti, D., Orecchio, B., Faccenna, C., Neri, G., 2010. Incipient extension along the active convergent margin of Nubia in Sicily: Cefalù-Etna seismic zone, Tectonics 29, TC4026, doi: 10.1029/2009TC002559.

Billi, A., Faccenna, C., Bellier, O., Minelli, L., Neri G., Piromallo, C., Presti, D., Scrocca, D., Serpelloni, E., 2011. Recent tectonic reorganization of the Nubia-Eurasia convergent boundary heading for the closure of the western Mediterranean. Bull. Soc. géol. France 182 (4), 279-303.

Bonardi, G., Giunta, G., Perrone, V., Russo, M., Zuppetta, A., Ciampo, G., 1980. Osservazioni sull'evoluzione dell'Arco Calabro-Peloritano nel Miocene inferiore: la Formazione di Stilo-Capo d'Orlando. Bollettino della Società Geologica Italiana, 99, pp. 365-393.

Bousquet J.C., 1977. Contribution à l'étude de la tectonique récente en Méditerranée: les données de la néotectonique dans l'arc de Gibraltar et dans l'arc tyrrhénien. In: «Structural history of the Mediterranean Basin». Technip, Paris, 199-214.

Bousquet J.C. and Lanzafame, G., 1995. Transition from Tyrrhenian basin extension to collisional tectonics: evidence of N-S compression during the recent Quaternary at Ustica (southern Tyrrhenian Sea, Italy). C.R. Acad. Sc. Paris, 321, II a, 781-787.

Bousquet J.C., Lanzafame, G., Paquin, C., 1988. Tectonic stresses and volcanism: in-situ stress

measurements and neotectonic investigations in the Etnean area (Italy). Tectonophysics, 149, 219-231, doi: 10.1016/0040-1951(88)90174-6.

Caccamo, D., Neri G., Saraò A., Wyss M., 1996. Estimate of stress directions by inversion of earthquake fault plane solutions in Sicily. Geophys. J. Int., 125, 3, 857-868, doi: 10.1111/j.1365-246X.1996.tb06029.x

Caputo, R., 1995. Evolution of orthogonal sets of coeval extension joints. Terra Nova 7, 479-490.

Caputo, R., 2010. Why joints are more abundant than faults. A conceptual model to estimate their ratio in layered carbonate rocks. J. Struct. Geol. 32, 1257-1270.

Carey-Gailhardis, E., Mercier, J.L., 1992. Regional state of stress, fault kinematics and adjustment of blocks in a fractured body of rock: application to the microseismicity of the Rhine Graben. J. Struct. Geol. 14, 1007-1017, doi: 10.1016/0191-8141(92)90032-R.

Carminati, E., Wortel, M.J.R., Spakman,W., Sabadini, R., 1998. The role of slab detachment processes in the opening of the Western-Central Mediterranean basins: some geological and geophysical evidence. Earth Planet. Sci. Lett. 160, 651-665, doi: 10.1016/S0012-821X(98)00118-6.

Catalano, S., Di Stefano A., 1997. Sollevamenti e tettogenesi pleistocenica lungo il margine tirrenico dei Monti Peloritani: integrazione dei dati geomorfologici, strutturali e biostratigrafici. Il Quaternario (Italian Journal of Quaternary Sciences) 10(2), 337-342.

Catalano, S., De Guidi, G., Monaco, C., Tortorici, G., Tortorici,L., 2003. Long-term behaviour of the Late Quaternary normal faults in the Straits of Messina area (Calabrian arc):structural and morphological constraints. Quat. Int. 101-102, 81-91.

Catalano, S., De Guidi, C., Monaco, C., Tortorici, G., Tortorici, L., 2008. Active faulting and seismicity along the Siculo-Calabrian Rift Zone (Southern Italy). Tectonophysics, 453, 177-192, doi: 10.1016/j.tecto.2007.05.008.

Cavazza, W., Blenkinsop, J., DeCelles, P., Patterson, R.T., Reinhardt, E., 1997. Stratigrafia e sedimentologia della sequenza sedimentaria oligocenico-quaternaria del bacino calabro-ionico. Boll. Soc. Geol. Ital. 116, 51-77.

Corti, G., Cuffaro, M., Doglioni, C., Innocenti, F. and Manetti, P., 2006. Coexisting geodynamic processes in the Sicily Channel, in Postcollisional Tectonics and Magmatism in the Mediterranean Region and Asia Edited by Y. Dilek and S. Pavlides, Spec. Pap. Geol. Soc. Am., 409, 83-96, doi: 10.1130/2006.2409(05).

Cristofolini, R., Patane, G., Puglisi, D., Rasa, R., Tranchina, A., 1977. Il basso versante nord-orientale dell'Etna nei dintorni di Piedimonte Etneo: studio geologico e morfostrutturale. Boll. Soc. Geol. Ital. 96, 695-712.

D'Agostino, N., and Selvaggi, G., 2004. Crustal motion along the Eurasia-Nubia plate boundary in the Calabrian Arc and Sicily and active extension in the Messina Straits from GPS measurements. J. Geophys. Res., 109, B11402, doi: 10.1029/2004JB002998.

D'Agostino, N., Avallone, A., Cheloni, D., D'Anastasio, E., Mantenuto, S., Selvaggi, G., 2008. Active tectonics of the Adriatic region from GPS and earthquake slip vectors. J. Geophys. Res., 113, B12413, doi: 10.1029/2008JB005860.

De Guidi, G., Catalano, S., Monaco, C., Tortorici, L., 2003. Morphological evidence of Holocene coseismic deformation in the Taormina region (NE Sicily). J. Geodyn. 36, 193-211, doi: 10.1016/S0264-3707(03)00047-4.

Doglioni, C., Innocenti, F., Mariotti, G., 2001. Why Mt. Etna?. Terra Nova 13, 25-31, doi: 10.1046/j.1365-3121.2001.00301.x.

Faccenna, C., Becker, T.W., Lucente, F.P., Jolivet, L., Rossetti, F., 2001. History of subduction and back-arc extension in the central Mediterranean. Geophys. J. Int. 145, 809-820, doi: 10.1046/j.0956-540x.2001.01435.x.

Faccenna, C., Molin, P., Orecchio, B., Olivetti, V., Bellier, O., Funiciello, F., Minelli, L., Piromallo, C., Billi, A., 2011. Topography of the Calabria subduction zone (southern Italy): Clues for the origin of Mt. Etna. Tectonics, 30, TC1003, doi: 10.1029/2010TC002694.

Falsaperla, S., Lanzafame, G., Longo, V., Spampinato, S., 1999. Regional stress field in the area of Stromboli (Italy): insights into structural data and crustal tectonic earthquakes. J. Volcanol. Geotherm. Res. 88, 147-166.

Ferranti, L., Monaco, C., Antonioli, F., Maschio, L., Kershaw, S., Verrubbi, V., 2007. The contribution of regional uplift and coseismic slip to the vertical crustal motion in the Messina Straits, southern Italy: Evidence from raised late Holocene shorelines. J. Geophys. Res., 112, B06401, doi: 10.1029/2006JB004473.

Ferranti, L., Oldow J. S., D'Argenio, B., Catalano, R., Lewis, D., Marsella, E., Avellone, G., Maschio, L., Pappone G., Pepe, F., Sulli, A., 2008. Active deformation in Southern Italy, Sicily and southern Sardinia from GPS velocities of the Peri-Tyrrhenian Geodetic Array (PTGA). Boll. Soc. Geol. Ital. 127(2), 299-316.

Finetti, I., Lentini, F., Carbone, S., Catalano, S., Del Ben, A., 1996. Il Sistema Appennino Meridionale-Arco Calabro-Sicilia nel mediterraneo centrale: studio geologico-geofisico. Mem. Soc. Geol. It., 115, 529-559.

Frepoli, A. and Amato, A., 2000. Spatial variation in stresses in peninsular Italy and Sicily from background seismicity. Tectonophysics 317, 109-124, doi: 10.1016/S0040-1951(99)00265-6.

Gephart, J. W. and Forsyth, W. D., 1984. An improved method for determining the regional stress tensor using earthquake focal mechanism data: Applications to the San Fernando earthquake sequence. J. Geophys. Res. 89, 9305-9320, doi: 10.1029/JB089iB11p09305.

Ghisetti, F., 1979. Relazione tra strutture e fasi trascorrenti e distensive lungo i sistemi Messina-Fiumefreddo, Tindari-Letojanni e Alia-Malvagna (Sicilia nord-orientale): uno studio microtettonico. Geol. Romana 18, 23-58.

Giammanco, S., Palano, M., Scaltrito, A., Scarfì, L., Sortino, F., 2008. Possible role of fluid

overpressure in the generation of earthquake swarms in active tectonic areas: the case of the Peloritani Mts. (Sicily, Italy). J. Volcanol. Geotherm. Res. 178, 795-806, doi: 10.1016/j.jvolgeores.2008.09.005.

Goes, S., Giardini, D., Jenny, S., Hollenstein, C., Kahle, H.G., Geiger, A., 2004. A recent tectonic reorganization in the south-central Mediterranean. Earth Planet. Sci. Lett. 226, 335-345, doi: 10.1016/j.epsl.2004.07.038.

Govers, R. and Wortel, M.J.R., 2005. Lithosphere tearing at STEP faults: response to edges of subduction zones. Earth Planet. Sci. Lett. 236,505-523, doi: 10.1016/j.epsl.2005.03.022 .

Hancock, P.L., AL-Kadhi, A., Barka, A.A., Bevan, T.G., 1987. Aspects of analyzing brittle structures. Annals Tecton. 1, 5-19.

Herring T.A., King, R.W., McClusky, S.C., 2009. Introduction to GAMIT/GLOBK, Release 10.4. Massachusetts Institute of Technology, Cambridge MA. 48 pp.

Holbrook, J. and Schumm, S.A, 1999. Geomorphic and sedimentary response of rivers to tectonic deformation: a brief review and critique of a tool for recognizing subtle epeirogenic deformation in modern and ancient settings. Tectonophysics 305, 287-306, doi: 10.1016/S0040-1951(99)00011-6.

Jenny, S., Goes, S., Giardini, D., Kahle, H.-G., 2006. Seismic potential of southern Italy. Tectonophysics, 415, 81-101, doi:10.1016/j.tecto.2005.12.003.

Langer, H., Raffaele, R., Scaltrito, A., Scarfi, L., 2007. Estimation of an optimum velocity model in the Peloritani Mountains-assessment of the variance of model parameters and variability of earthquake locations. Geophys. J. Int. 170 (3), 1151-1164, doi: 10.1111/j.1365-246X.2007.03459.x.

Lanzafame, G., and Bousquet, J.C., 1997. The Maltese escarpment and its extension from Mt. Etna to the Aeolian Islands (Sicily): importance and evolution of a lithosphere discontinuity. Acta Vulcanol. 9, 113-120.

Lavecchia, G., F. Ferrarini, R. de Nardis, F. Visini, Barbano, M. S. 2007. Active thrusting as a possible seismogenic source in Sicily (southern Italy): Some insights from integrated structural-kinematic and seismological data. ectonophysics, 445, 145-167, doi:10.1016/j.tecto.2007.07.007.

Lentini, F., Catalano, S., Carbone, S., 2000. Carta geologica della Provincia di Messina, Note Illustrative, 70 pp. SELCA, Florence, Italy.

Lund, B. and Townend, J., 2007. Calculating horizontal stress orientations with full or partial knowledge of the tectonic stress tensor. Geophys. J. Int. 270, 1328-1335, doi: 10.1111/j.1365-246X.2007.03468.x.

Malinverno, A. and Ryan, W.B.F., 1986. Extension in the Tyrrhenian Sea and shortening in the Apennines as result of arc migration driven by sinking of the lithosphere. Tectonics 5(2), 227-245, doi: 10.1029/TC005i002p00227.

Mattia, M., Palano, M., Bruno, V., Cannavò, F., 2009. Crustal motion along the Calabro-

Peloritano Arc as imaged by twelve years of measurements on a dense GPS network. Tectonophysics, 476, 528-537, doi: 10.1016/j.tecto.2009.06.006.

Mattia, M., Palano, M., Bruno, V., Cannavò, F., Bonaccorso, A., Gresta, S., 2008. Tectonic features of the Lipari-Vulcano complex (Aeolian archipelago, Italy) from 10 years (1996-2006) of GPS data. Terra Nova 20, 370-377, doi: 10.1111/j.1365-3121.2008.00830.

Michael, A. J., 1987. Use of focal mechanisms to determine stress: A control study. J. Geophys. Res., 92, 357-368, doi: 10.1029/JB092iB01p00357.

Monaco, C., Mazzoli, S., Tortorici, L., 1996. Active thrust tectonics in western Sicily (southern Italy): the 1968 Belice earthquake sequence. Terra Nova 8, 372-381, doi: 10.1111/j.1365-3121.1996.tb00570.x.

Montone, P., Mariucci, M.T., Pondrelli, S., Amato, A., 2004. An improbe stress map for Italy and surrounding regions (Central Mediterranean). J. Geophys. Res., 109, B10410, doi: 10.1029/2003JB002703.

Neri, G., Barberi, G., Oliva, G., Orecchio, B., 2005. Spatial variations of seismogenic stress orientations in Sicily, South Italy. Phys. Earth Planet. In. 148, 175-191, doi: 10.1016/j.pepi.2004.08.009.

Nicolich, R., Laigle, M., Hirn, A., Cernobori, L., Gallard, J., 2000. Crustal structure of the Ionian margin of Sicily: Etna volcano in the frame of regional evolution. Tectonophysics 329, 121-139, doi:10.1016/S0040-1951(00)00192-X.

Ogniben, L., 1960. Nota illustrativa dello schema geologico della Sicilia nord-orientale. Riv. Min. Sicil. 64-65, 183-212.

Palano, M., Rossi, M., Cannavò, F., Bruno, V., Aloisi, M., Pellegrino, D., Pulvirenti, M., Siligato, G., Mattia, M., 2010. Etn@ref: a geodetic reference frame for Mt. Etna GPS networks. Ann. Geophys., 53 (4), doi: 10.4401/ag-4879.

Palano, M., Cannavò, F., Ferranti, F., Mattia, M., Mazzella., M. E., 2011. Strain and stress fields in the Southern Apennines (Italy) constrained by geodetic, seismological and borehole data. Geophys. J. Int. 187, 1270-1282, doi: 10.1111/j.1365-246X.2011.05234.x.

Palano, M., Ferranti, L. Monaco, C. Mattia, M., Aloisi, M. Bruno, V., Cannavò, F., Siligato, G., 2012. GPS velocity and strain fields in Sicily and southern Calabria, Italy: Updated geodetic constraints on tectonic block interaction in the central Mediterranean. J. Geophys. Res., 117, B07401, doi:10.1029/2012JB009254.

Parker, R. L., and McNutt, M. K., 1980. Statistics for the one-norm misfit measure. J. Geophys. Res. 85, 4429-4430, doi: 10.1029/JB085iB08p04429.

Patacca, E., Sartori, R., Scandone, P., 1990. Tyrrhenian basin and Apenninic arcs: Kinematic relations since late Tortonian times. Mem. Soc. Geol. Ital. 45, 425-451.

Polonia, A., Torelli, L., Mussoni, P., Gasperini, L., Artoni, A., Klaeschen, D., 2011. The Calabrian Arc subduction complex in the Ionian Sea: Regional architecture, active deformation, and seismic hazard. Tectonics, 30, TC5018, doi:10.1029/2010TC002821.

Pondrelli, S., Salimbeni, S., Ekström, G., Morelli, A., Gasperini, P., Vannucci, G., 2006. The Italian CMT dataset from 1977 to the present. Phys. Earth Planet. Interiors 159(3-4), 286-303, doi: 10.1016/j.pepi.2006.07.008.

Puglisi, G., Aloisi, M., Mostaccio, A., Puglisi, B., 1999. Misure GPS sull'allineamento strutturale Eolie-Tindari-Giardini. GNGTS atti del 18° Convegno Nazionale 08/18, http://www2.ogs.trieste.it/gngts/gngts/convegniprecedenti/1999/media/contents/pdf/8_18.pdf

Reasenberg, P., Oppenheimer, D., 1985. FPFIT, FPPLOT, and FPPAGE: FORTRAN computer programs for calculating and displaying fault plane solutions. U.S. Geol. Surv. Open File Rep. 85/739, 109 pp.

Scandone, P., Pattacca, E., Radoicic, R., Ryan, W.B.F., Cita, M.B., Rawson, M., Chezar, H., Mackenzie, J. and Rossi, S., 1981. Mesozoic and Cainozoic rocks from Malta escarpment (Central Mediterranean). Am. Assoc. Petrol. Geol. Bull., 65: 1299-1319.

Scarfì, L., Langer, H., Scaltrito, A., 2005. Relocation of microearthquake swarms in the Peloritani mountains – implications on the interpretation of seismotectonic patterns in NE Sicily, Italy. Geophys. J. Int. 163, 225-237, doi: 10.1111/j.1365-246X.2005.02720.x.

Scarfì, L., Langer, H., Scaltrito, A., 2009. Seismicity, seismotectonics and crustal velocity structure of the Messina Strait (Italy). Phys. Earth Planet. In., 177, 65-78, doi: 10.1016/j.pepi.2009.07.010.

Stewart, I., Cundy, A., Kershaw, S., Firth, C., 1997. Holocene coastal uplift in the Taormina area, northeastern Sicily: implications for the southern prolongation of the Calabrian seismogenic belt. J. Geodyn. 24, 37-50, doi: 10.1016/S0264-3707(97)00012-4.

Tortorici, L., Cocina, O., Monaco, C., Tansi, C., 1995. Recent and active tectonics of the Calabrian Arc (Southern Italy). Tectonophysics 243, 37-55, doi: 10.1016/0040-1951(94)00190-K.

Vecchia, O., 1963. The gravity field of Italy: a geotectonic interpretation. Boll. Geod. Sc. Affini 22, 1-19.

Westaway, R., 1990. Present-day kinematics of the plate boundary zone between Africa and Europe, from the Azores to Aegean. Earth Planet. Sci. Lett. 96, 392-406, doi:10.1016/0012-821X(90)90015-P.

Wortel, M. J. R., and Spakman W., 2000. Subduction and slab detachment in the Mediterranean-Carpathian region. Science, 290, 1910-1917, doi: 10.1126/science.290.5498.1910.

Wyss, M., Liang, B., Tanigawa, W.R., Xiaoping, W., 1992. Comparison of orientations of stress and strain tensor based on fault plane solutions in Kaoiki, Hawaii. J. Geophys. Res. 97, 4769-4790, doi: 10.1029/91JB02968.

Figure captions

Fig. 1. a) Regional tectonic map of southern Italy. Abbreviations in the legend are as follows: CPU, Calabro-Peloritan Arc Units; SMU, Sicilian-Maghrebian Units; V, Volcanic rocks; HFU, Hyblean Foreland Units. 1) main thrust fronts; 2) main faults; 3) Sh_{min} stress orientations from Neri et al. (2005) and Billi et al. (2010); 4) SH_{max} stress orientations from Bousquet and Lanzafame (1995) and Neri et al. (2005); 5) SH_{max} stress orientations computed from single focal mechanisms as reported in Montone et al. (2004) and Pondrelli et al. (2006). Other abbreviations are: ATL, Aeolian-Tindari-Letojanni fault system; Ce, Cefalù; PC, Peloritani chain; NM, Nebrodi Mts.; MtE, Mt. Etna; HMFS, Hyblean-Maltese fault system. b) IGS stations used in this work. c) Simplified tectonic map of north-eastern Sicily and southern Calabria. Permanent seismic stations are reported as white triangles; GPS benchmarks are reported as black circles; common stations (both GPS and seismic) are reported as white stars. Abbreviations are: TFL, Tindari fault line; CT, Capo Tindari. Blue box shows the area represented in Fig.2.

Fig. 2. Simplified structural and geological map of the investigated area. 1: Holocene alluvial and talus deposits; 2: Pliocene-Pleistocene marine and continental sediments covering the thrust-chain; 3: Cretaceous-Miocene sedimentary units of the thrust-chain; 4: Hercynian metamorphic units of the thrust-chain; 5: fault; 6: tectonic analysis sites; 7: extension direction obtained by (a) numerical method, (b) graphic methods, (c) qualitative observations on large faults. Numbers and arrows on the map indicate measurement sites and results of structural analysis respectively.

Fig. 3. a) GPS velocities and 95% confidence ellipses in a fixed Eurasian frame. A diagram showing the relationships between vector displacement azimuths (computed for each pair of stations located across the analyzed fault according to a Monte Carlo resampling) and the local strike of TFL (dashed gray line) is also reported. b) Greatest extensional (in white) and shortening (in black)

horizontal strain-rates computed for the investigated area. TFL is shown as a thicker line.

Fig. 4. Map (a) and depth W-E profile (b) showing hypocenter location for more than 1000 earthquakes from the INGV-CT catalogue (http://www.ct.ingv.it/Sismologia/analisti/default.asp), recorded between 1999 and 2010. Abbreviations are as follows: CC, Capo Calavà; No, Novara di Sicilia; CT, Capo Tindari; Ca, Castroreale.

Fig. 5. a) Lower hemisphere, equal area projection for the 69 fault plane solutions computed for the investigated area and used in this study (see Table 1 for more details). A1, A2, A3, A4 represent the areas in which FPs were grouped, by taking into account their (1) kinematics, (2) focal depths and (3) epicentral distribution with respect to TFL. b) Stress tensor resulting from the inversion of the FPs of the events located in areas A1, A2 and A3. Best-fit and 95% confidence are reported as white symbols and gray symbols, respectively. Histograms show the uncertainty in the stress ratio R. N is the number of FPs used to calculate the tensor; F is the average misfit to the best-fit tensor. Plunge and trend of the three main stress axes and Sh_{min} orientation are also reported. A4 area was excluded from the stress tensor inversion (see text for details).

Fig. 6. Near the coast, at 3.8 km south of Capo Tindari (Site 1 in Fig. 2). This normal fault cuts the metamorphic rocks of the chain and the current fluvial-coast deposits. The movement plane, striking N 15-30°E and dipping 60° E, shows double sets of striations with extensional dip-slip striae (pitch 70° N) that overprint the right-normal strike-slip ones (pitch 30° S). The measured planes and striae indicate two different directions of extension (see Fig. 2 and Tab. 2), which are ENE-WSW (dip-slip) and NNW-SSE (right-strike slip) oriented, and not compatible with each other.

Fig. 7. Immediately west of the Tripi cemetery (Site 2 in Fig. 2). The Tindari fault line shows the

greatest morphological expression. The main fault attains an attitude of N 140°E, 70°E, and normally dissects the range displaying a very large triangular facet up to 250 m high (a). A metric thickness of cataclastic rocks covers the movement plane (b). At the tectonic escarpment base, the continuous fault activity has favoured the deposition of a well-developed Holocene piedmont talus (c), which in turn has been cut by the renewed activity of the structure. In contrast with the apparent normal dynamics of the fault, the slickenlines measured at the main movement plane and at the secondary planes that deform the talus, the cataclastics and the bedrock (stereographic projections, Schmidt net in a; see Tab. 2), indicate that the dominant vertical movement trends (N 40°E extension) are accompanied by evident dislocation traces with marked right-strike slip component (N 125°E extension).

Fig. 8. The confluence of the Mazzarrà and Tripi rivers seen from north-east (a). After having dislocated the Tripi talus deposit (C in Fig. 6), just southward the fault displaces the current Mazzarà river flood plain. Westwards, at the rising footwall, the active dislocation allowed: (1) the development of an alluvial fan that does not relate to any hydraulic process; (2) the Tripi river to flow in meander (α), contrasting the marked slope of the river bed; (3) erosion to cut and bring the fan deposits to the surface. The latter consists of rounded elements, well imbricated by the current flow, and of numerous rounded fragments of late-Roman terracotta (1500 yrs old; see arrows in B and C). In the eastern side of the fault (downthrown), some stable 70 year-old wells (D), neither eroded or flooded, can be observed: these testify that in this period, the distension process of the fault system essentially acted by means of the footwall lift, which at the Tripi river has been about 3 m in the last 1500 years.

Fig. 9. The Rocca Novara horst (Site 3 in Fig. 2) as seen from north-east (A). 1: Hercyanian phyllites and discontinuous patches of red conglomerates; 2: Tithonian limestones; 3: Cretaceous varicolored clays; 4: Langhian calcarenites of Floresta. The yellow arrows indicate the Holocene

rock flow (α) which, at Serro Rosano (α'), is dissected and raised by 40-50 m by the easternmost horst fault (φ). At Santa Croce Mount, northeastern end of the horst, a free face at the base of a normal fault plane (NW-SE, 70° NE) testifies to recent motions (B; Site 4 in Fig. 2). The geometry and kinematics of this main fault and of the structurally associated small faults (stereographic projections, Schmidt net in C) reveal prevalent normal motion (N 66°E extension) and less marked extensional displacement with high right-lateral components (N 130°E extension). See Table 2 and Fig. 2.

Fig. 10. On the right bank of the Brandino river (Site 5 in Fig. 2), the extensional fault (N 120-130° E-trending, 40-50° SW dipping) offsets a little ridge sculpted in the Holocene piedmont deposits (A). The recognition of the same elements from one side of the discontinuity to the other, allows tracking the motion vector on the fault plane, showing that the discontinuity (the Holocenic piedmont was first deposited, later shaped by erosion and finally displaced by the fault) has recently been controlled by an extensional NNW-SSE-trending strength system, acting according to a left-normal kinematics (pitch 30° SE). A little southward along the Blandino river left bank (Site 6 in Fig. 2), the normal fault (B; N10°E, dip 45° W, pitch 65° S) offsets the vegetated soil and the low-grade metamorphic substrate by about 1 m, indicating the current almost ENE-WSW extension activity.

Fig. 11. The Giarra fault as seen from SE (Site 7 in Fig. 2). The large normal fault, N 43°E-oriented, dipping 65-70° to SE, pitch 65-70° SW, cuts and dislocates the metamorphic rocks by 30-40 m. The prominent and fresh morpho-structural feature of the deformation, not yet degraded by erosion, clearly reflects the recent-Holocene age of the fault activity and of the resulting ~NW-SE extension (Tab. 2).

Fig. 12. Map of the minimum compressive horizontal stress (Sh_{min}) computed by (1) seismic and

(3) geologic data and the maximum extensional strain-rates (ε_{Hmax}) computed by (2) geodetic data.

Table captions

Table 1. Selected fault plane solutions. Date is in format day-month-year; O.T. = origin time (hour and minute); latitude north and longitude east; depth in km; M = magnitude.

Table 2. Results of structural analysis on the studied sites. All measurements refer to Holocene-historical-present day fault motions.

Supplementary materials

Table S1. Site code, geodetic coordinates, east and north velocity components referred to a fixed a fixed Eurasian frame (Mattia et al., 2008) for all GPS stations included in the processing. For each site, associated errors (95% of confidence), the correlation between the east and north components of velocity (RHO) and the observation history, are also reported.

Table S2. Principal strain-rates and 1σ uncertainties computed for each quadrilateral reported in Fig. 3b. Positive and negative values represent extension and contraction respectively (φ is the azimuth of ε_{Hmax}).

Table 1

Event ID	Date	O.T.	Lat. (°E)	Long. (°N)	M	Depth (km)	Plane 1			Plane 2			Note
							Strike (°)	Dip (°)	Rake (°)	Strike (°)	Dip (°)	Rake (°)	
01	28/08/1999	18:20	38.022	15.058	2.7	16.60	345	30	-120	199	64	-74	A3
02	30/01/2000	11:52	38.286	15.184	2.6	7.80	240	85	30	147	60	174	A4
03	29/05/2000	14:25	38.138	15.136	3.0	9.44	5	40	-110	210	53	-74	A5
04	02/09/2000	23:51	38.138	15.069	2.7	4.61	30	55	-90	210	35	-90	A5
05	08/05/2001	03:53	38.154	14.945	3.3	8.35	150	55	-40	266	58	-137	A2
06	25/06/2001	15:45	38.173	15.199	2.8	9.42	355	50	-120	217	48	-59	A5
07	26/11/2001	15:48	38.169	15.036	2.8	13.96	45	30	-90	225	60	-90	A5
08	29/11/2001	05:27	38.069	15.126	2.7	7.20	315	45	-120	174	52	-64	A5
09	04/12/2001	09:01	37.969	14.708	2.9	13.77	25	60	-50	146	48	-138	A1
10	25/12/2001	15:53	37.938	14.780	3.2	5.49	120	55	80	317	36	104	A1
11	29/12/2001	16:22	37.973	14.786	2.8	3.48	185	75	120	299	33	28	A1
12	22/01/2002	22:54	37.988	14.768	2.6	11.43	30	55	-60	165	45	-125	A1
13	29/07/2002	01:54	38.122	15.143	2.5	11.88	5	45	-120	224	52	-64	A5
14	21/08/2002	03:54	38.286	15.016	2.5	14.18	355	45	-160	251	76	-47	A4
15	27/08/2002	17:10	38.070	15.111	2.1	11.63	45	55	-70	193	40	-116	A5
16	20/11/2002	02:31	38.204	14.805	3.5	17.36	15	65	-20	114	72	-154	A2
17	17/12/2002	23:13	38.137	15.121	2.5	14.31	55	50	-90	235	40	-90	A5
18	06/03/2003	02:06	38.018	14.758	2.6	1.63	10	65	-120	244	38	-43	A1
19	21/04/2003	15:45	38.113	15.215	2.6	8.15	35	30	-100	227	61	-84	A5
20	21/04/2003	16:02	38.117	15.204	2.4	9.95	35	30	-100	227	61	-84	A5
21	11/06/2003	08:32	38.110	15.214	2.8	10.40	35	30	-100	227	61	-84	A5
22	13/06/2003	23:19	38.181	15.090	3.2	6.73	60	90	30	330	60	180	A4
23	01/07/2003	23:49	38.121	15.234	3.1	9.00	45	55	-85	216	35	-97	A5
24	27/11/2003	01:01	37.987	14.790	2.8	12.13	75	40	-110	280	53	-74	A1
25	02/12/2003	04:59	38.232	15.130	2.7	10.00	95	70	-90	275	20	-90	A5
26	23/07/2004	12:32	38.129	14.955	2.0	20.08	160	50	-60	298	48	-121	A2
27	27/07/2004	10:43	38.122	14.947	2.2	18.86	110	35	-70	266	57	-103	A2
28	29/07/2004	17:33	38.133	14.955	2.3	21.93	40	25	-100	231	65	-85	A2
29	02/08/2004	16:38	38.118	14.924	2.5	26.48	115	40	-50	247	61	-119	A2
30	02/08/2004	19:51	38.124	14.963	2.1	19.54	75	35	-70	231	57	-103	A2
31	08/08/2004	08:09	38.209	15.055	2.5	16.34	55	35	-10	153	84	-125	A4
32	03/01/2005	20:09	38.158	15.147	2.7	9.65	70	55	-70	218	40	-116	A5
33	22/03/2005	18:44	38.127	15.143	2.6	8.66	70	40	-70	225	53	-106	A5
34	10/01/2006	22:12	38.120	15.228	2.3	11.70	35	30	-90	215	60	-90	A5
35	27/02/2006	04:34	38.137	15.204	4.2	10.10	60	35	-120	275	60	-71	A5
36	01/04/2006	23:06	38.047	15.051	2.2	7.81	60	40	-110	265	53	-74	A3

37	01/07/2006	15:03	38.114	15.205	2.3	11.61	70	45	-110	277	48	-71	A5
38	02/07/2006	17:51	38.125	15.120	2.2	17.43	40	40	-80	207	51	-98	A5
39	20/09/2006	16:16	38.088	15.130	2.5	14.08	90	50	-70	240	44	-113	A5
40	04/11/2006	05:59	38.035	15.043	3.1	14.14	160	70	-60	281	36	-144	A3
41	01/01/2007	07:58	38.169	14.901	2.7	27.85	155	55	120	290	45	55	A2
42	02/01/2007	13:30	38.150	14.950	2.7	17.30	160	65	110	299	32	54	A2
43	03/06/2007	14:11	38.059	14.981	2.3	12.66	70	50	-80	235	41	-101	A3
44	18/08/2007	14:04	38.203	15.174	4.2	13.63	45	35	-70	201	57	-103	A5
45	18/08/2007	14:21	38.188	15.166	3.2	14.36	30	55	-100	227	36	-76	A5
46	24/08/2007	01:34	38.187	15.174	2.3	10.71	35	55	-100	232	36	-76	A5
47	24/08/2007	15:22	38.147	15.173	2.3	11.53	30	55	-90	210	35	-90	A5
48	07/09/2007	04:40	38.186	15.165	2.0	11.57	55	60	-70	199	36	-121	A5
49	13/09/2007	15:19	38.187	15.156	2.8	13.75	70	55	-50	194	51	-133	A5
50	14/09/2007	01:06	38.238	15.067	3.2	12.43	65	90	40	335	50	180	A4
51	27/10/2007	08:39	37.947	15.122	2.9	8.19	120	40	-90	300	50	-90	A3
52	10/03/2008	11:23	37.985	15.128	3.0	6.42	115	50	-70	265	44	-113	A3
53	28/04/2008	17:27	38.140	15.129	2.5	12.84	20	40	-110	225	53	-74	A5
54	02/07/2008	02:17	38.076	15.035	2.4	20.72	175	55	-40	291	58	-137	A3
55	14/07/2008	04:12	38.117	15.181	2.2	10.29	40	50	-90	220	40	-90	A5
56	16/07/2008	07:44	38.094	15.088	2.6	8.89	60	55	-90	240	35	-90	A5
57	01/09/2008	14:45	37.988	15.098	3.0	9.50	20	45	-110	227	48	-71	A3
58	02/09/2008	09:16	37.989	15.103	3.3	9.60	15	45	-100	209	46	-80	A3
59	27/10/2008	10:55	38.120	15.166	3.8	12.60	55	45	-80	221	46	-100	A5
60	11/11/2008	13:31	37.997	15.168	2.3	10.17	110	35	-90	290	55	-90	A5
61	01/03/2009	20:57	38.134	14.941	3.0	19.50	140	50	-180	49	89	-40	A2
62	27/04/2009	09:42	38.044	15.109	3.3	9.83	35	55	-100	232	36	-76	A3
63	27/05/2009	05:25	38.030	15.083	2.4	11.24	40	40	-90	220	50	-90	A3
64	18/06/2009	14:40	38.029	15.050	2.3	11.90	105	55	-70	253	40	-116	A3
65	12/09/2009	08:23	38.088	15.168	2.1	34.90	65	45	-150	313	69	-49	A5
66	25/10/2009	17:50	38.236	15.114	2.7	14.59	80	70	40	334	53	155	A4
67	12/02/2010	06:46	38.110	15.151	3.0	10.10	40	55	-90	220	35	-90	A5
68	23/04/2010	20:05	38.274	15.033	2.6	12.78	220	85	-30	313	60	-174	A4
69	06/06/2010	16:49	38.209	15.123	3.7	14.85	60	75	30	322	61	163	A4

Table 2.

Sampling Site	Analysis Method	Extension Orientation	Motion	R ratio
1. Costal zone	graphic	ENE-WSW NNW-SSE	dip-slip right strike-slip	
2. Tripi	numerical	N40°E N125°E	dip-slip right strike-slip	0.90
3. Rocca Novara	qualitative observation	ENE-WSW	dip-slip	
4. Santa Croce	numerical	N66°E N130°E	dip-slip right strike-slip	0.88
5. Brandino 1	graphic	NNW-SSE	left strike-slip	
6. Brandino 2	graphic	ENE-WSW	dip-slip	
7. Giarra	qualitative observation	NW-SE	dip-slip	

Figure 1

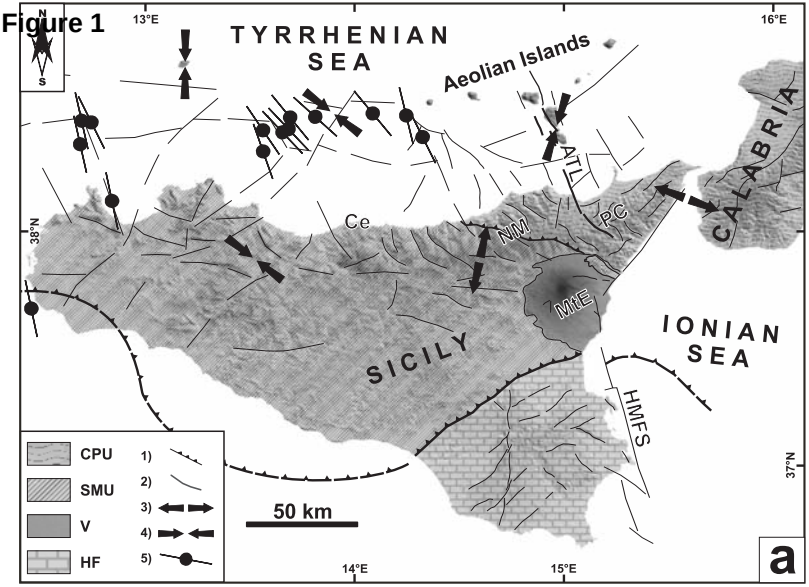
13°E
16°E
TYRRHENIAN SEA
Aeolian Islands
ATL
CALABRIA
Ce
NM
PC
38°N
MtE
SICILY
IONIAN SEA
HMFS
37°N
CPU
SMU
V
HF
1)
2)
3)
4)
5)
50 km
14°E
15°E
a


EURASIA
GRAZ
MEDI
GRAS
AJAC
Tyrrhenian chain
Tyrrhenian Sea
MATE
CAGL
Apennine - Maghrebian chain
NOTO
NOT1
AFRICA
LAMP
b

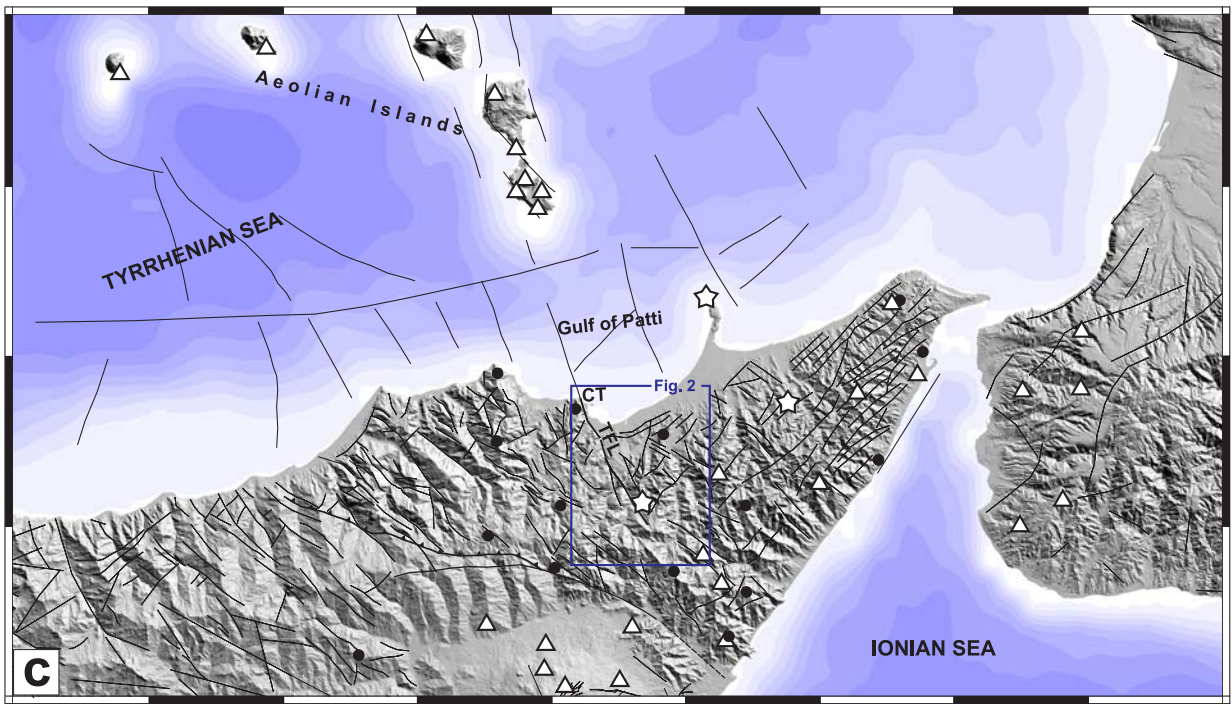
Aeolian Islands
TYRRHENIAN SEA
Gulf of Patti
CT
Fig. 2
TFL
IONIAN SEA
c
18.40°
38.00°
14.20°
14.60°
15.00°
15.40°
15.80°

Figure 2

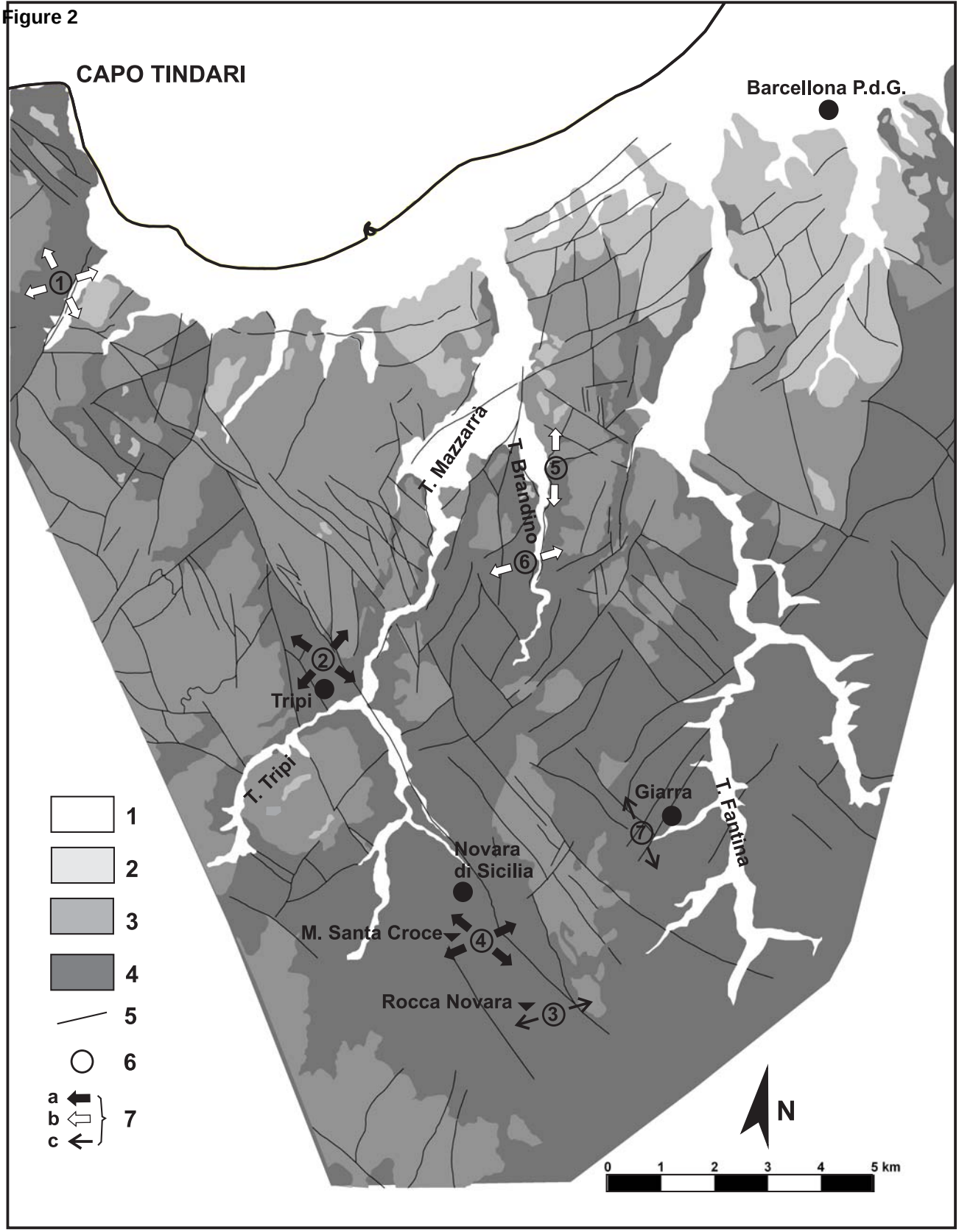
CAPO TINDARI
Barcellona P.d.G.
T. Mazzarrà
T. Brandino
Tripi
T. Tripi
Giarra
T. Fantina
Novara di Sicilia
M. Santa Croce
Rocca Novara
1
2
3
4
5
6
a
b
c
7
N
0 1 2 3 4 5 km

Figure 3

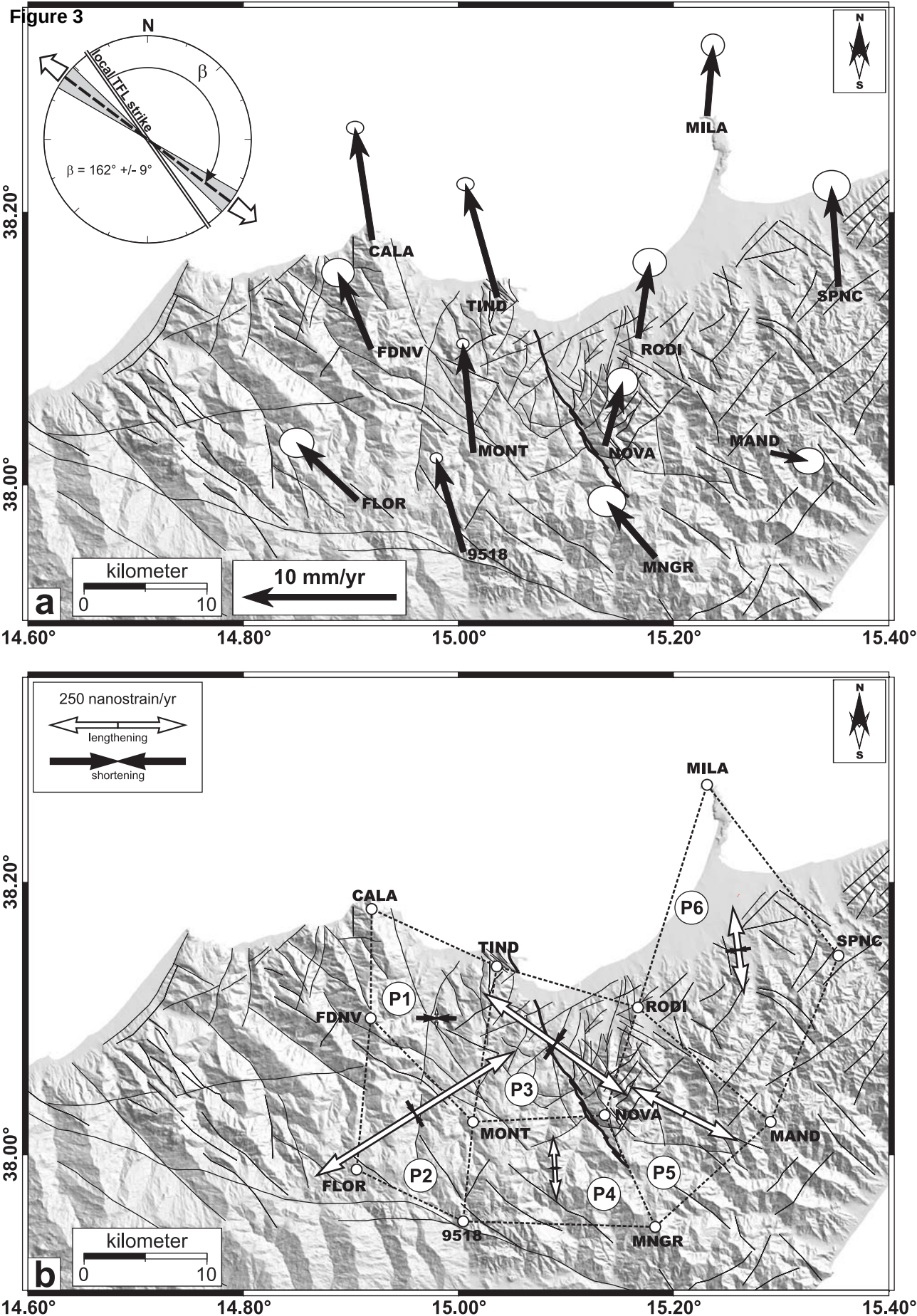
N
local TFL strike
β
β = 162° +/- 9°
N
S
MILA
CALA
TIND
SPNC
FDNV
RODI
MONT
NOVA
MAND
FLOR
9518
MNGR
kilometer
0
10
10 mm/yr
a
38.20°
38.00°
14.60°
14.80°
15.00°
15.20°
15.40°
250 nanostrain/yr
lengthening
shortening
N
S
MILA
CALA
TIND
SPNC
P6
P1
FDNV
RODI
P3
NOVA
MONT
MAND
P2
P5
P4
FLOR
9518
MNGR
kilometer
0
10
b
38.20°
38.00°
14.60°
14.80°
15.00°
15.20°
15.40°

Figure 4

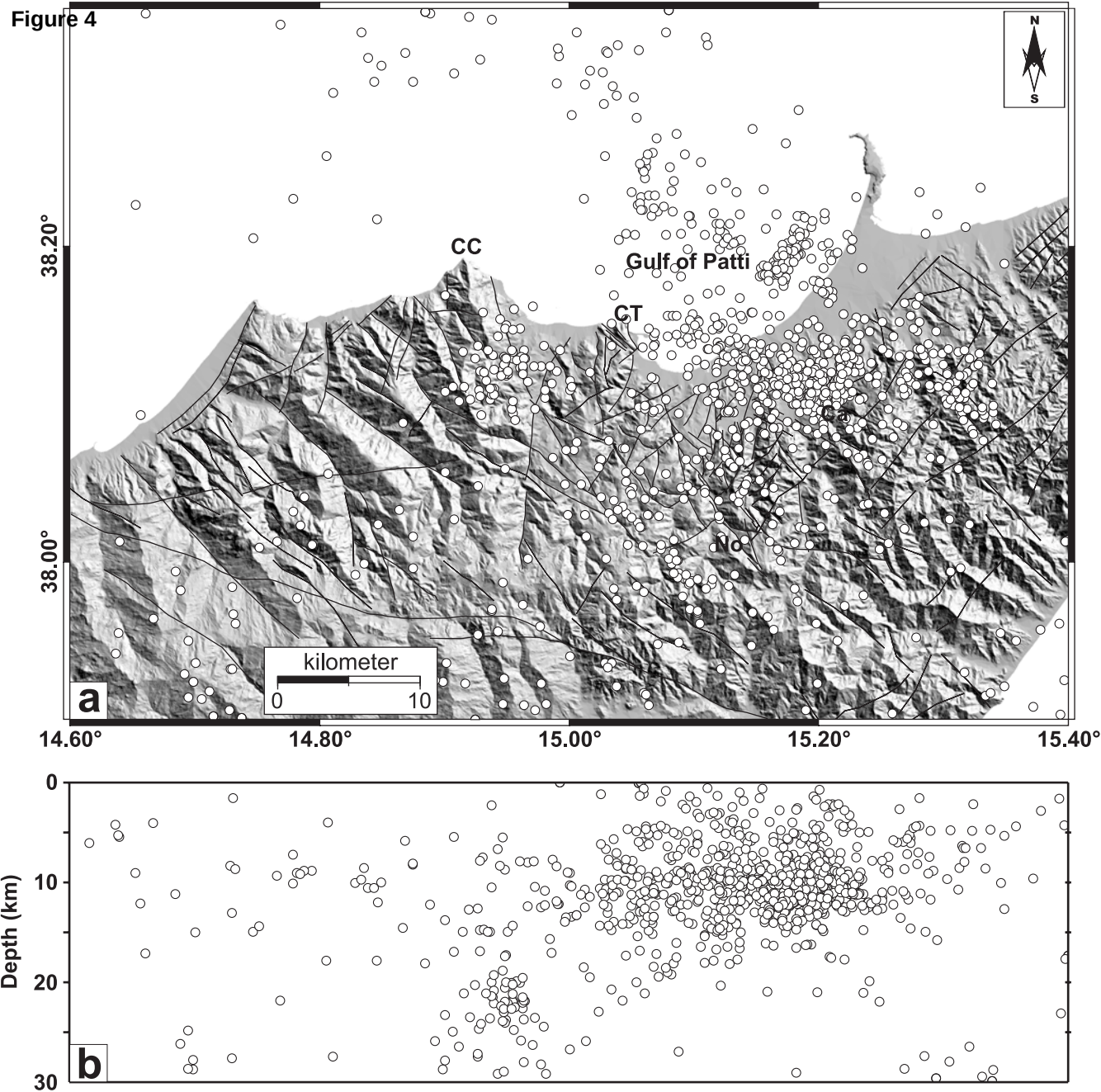
N
S
38.20°
38.00°
CC
Gulf of Patti
CT
kilometer
0
10
a
14.60°
14.80°
15.00°
15.20°
15.40°
Depth (km)
0
10
20
30
b

Figure 5

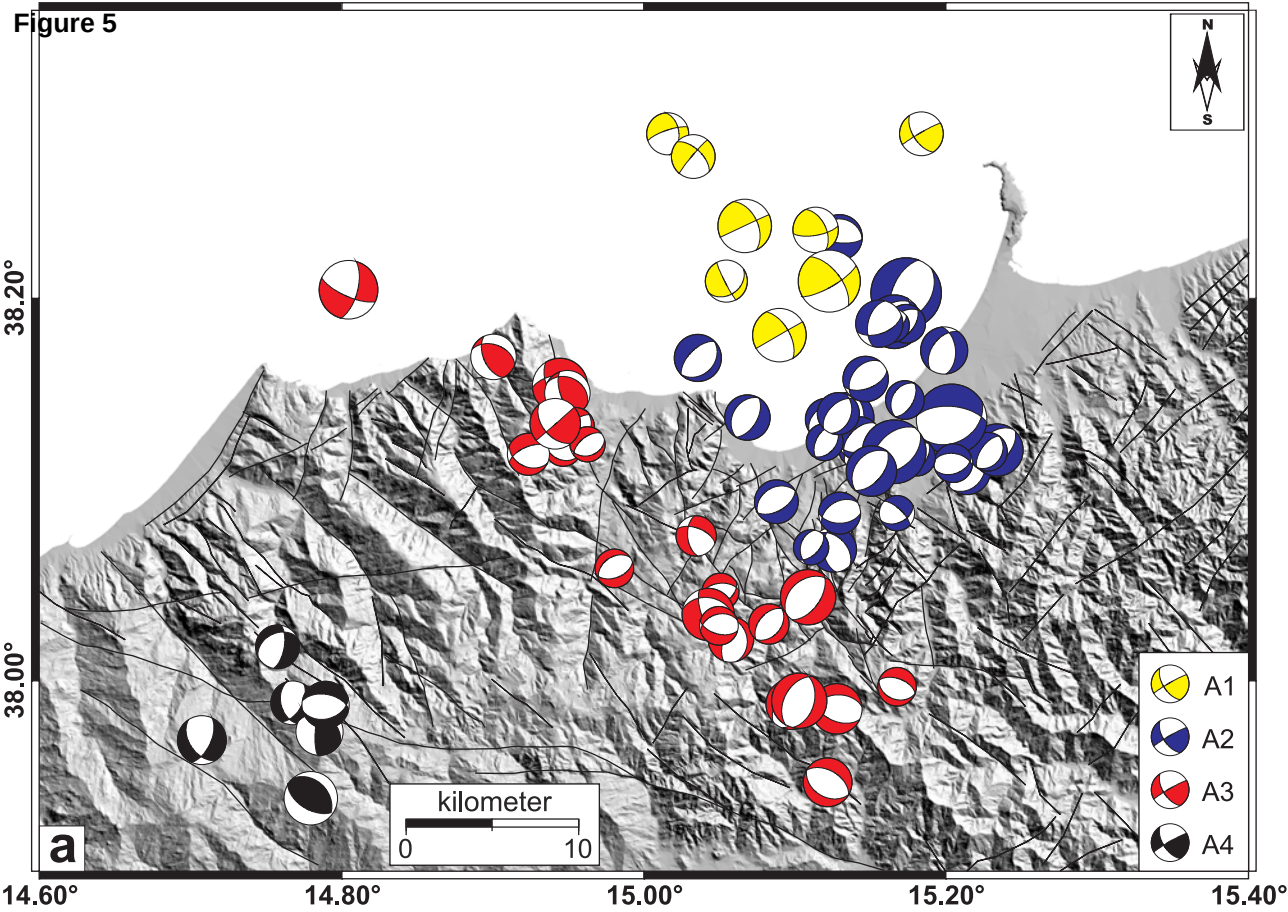

All FPSs	A1	A2	A3
N FPSs = 69	N FPSs = 8	N FPSs = 32	N FPSs = 18
F = 7.6	F = 1.4	F = 3.0	F = 3.4
R = 0.55	R = 0.5	R = 0.55	R = 0.65
σ_1 = 62/196	σ_1 = 14/190	σ_1 = 82/136	σ_1 = 60/150
σ_2 = 28/25	σ_2 = 60/74	σ_2 = 1/40	σ_2 = 10/257
σ_3 = 4/293	σ_3 = 26/287	σ_3 = 8/310	σ_3 = 28/353
Sh_{min} = 112°	Sh_{min} = 102°	Sh_{min} = 130°	Sh_{min} = 11°
Stress regime = NF	Stress regime = SS	Stress regime = NF	Stress regime = NF

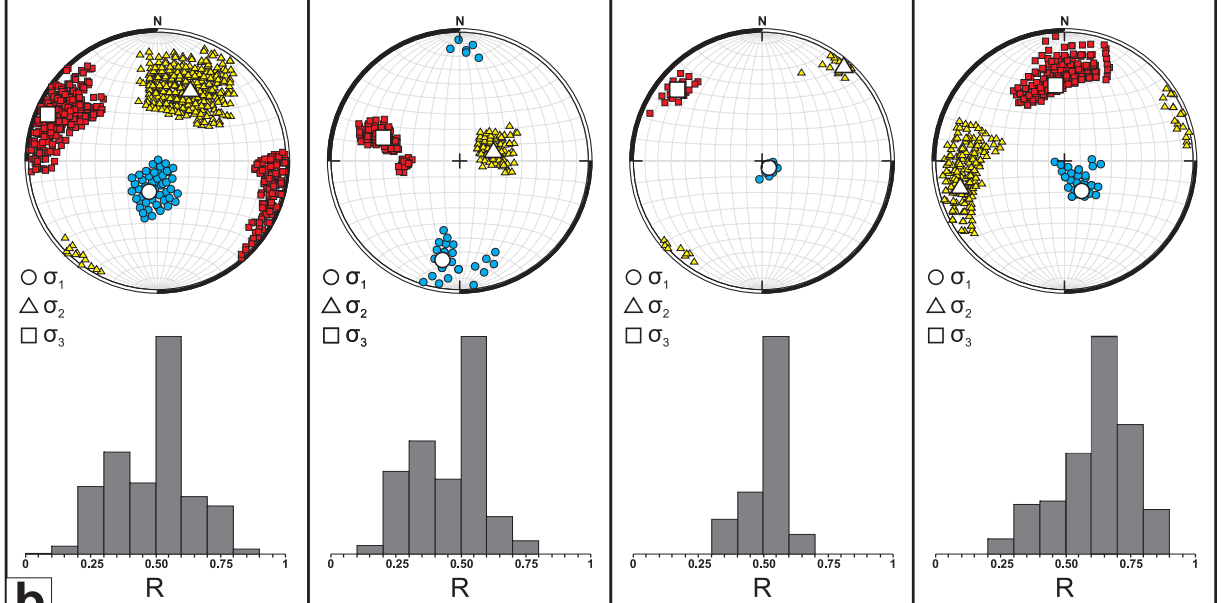

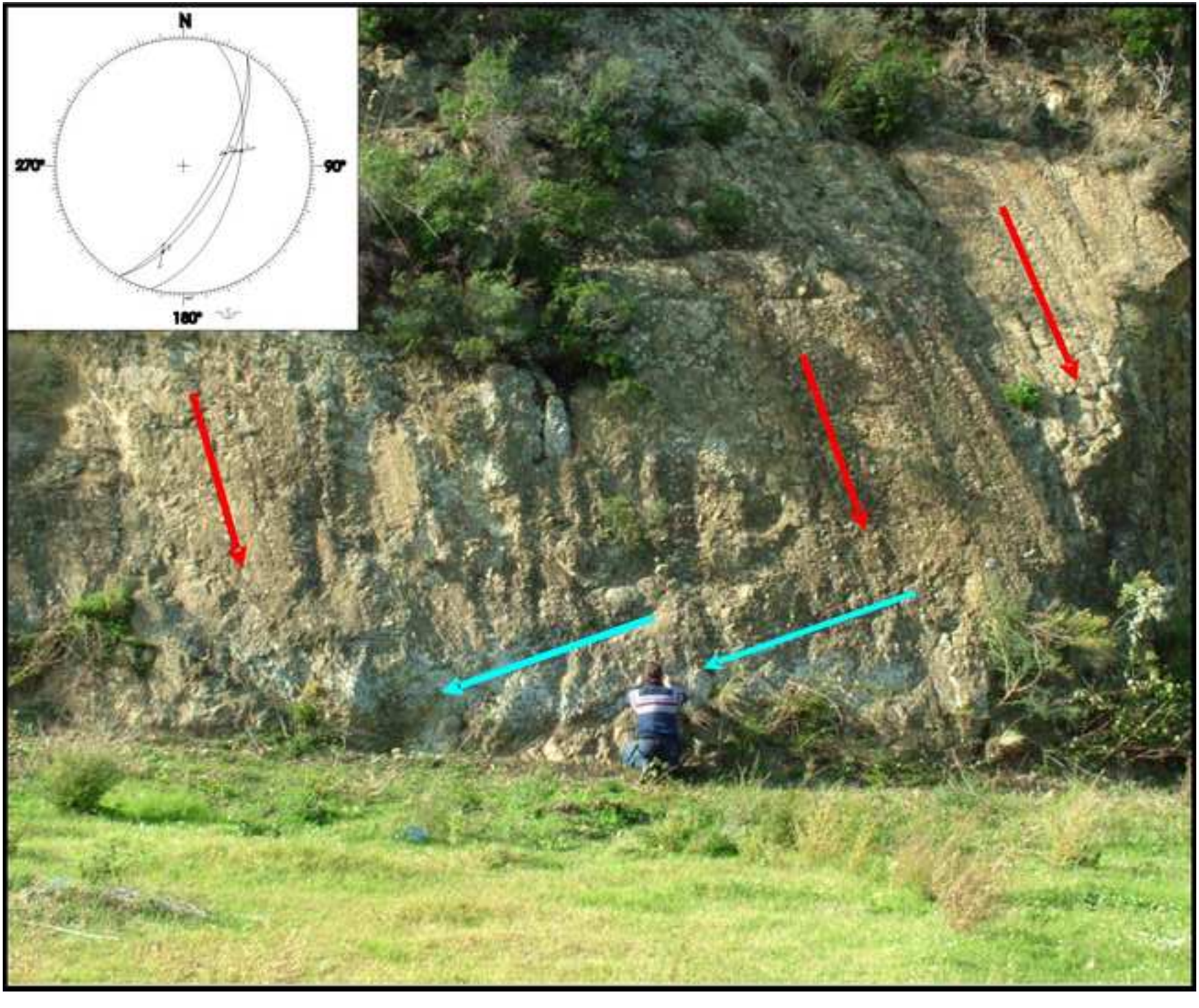
N
270°
90°
180°

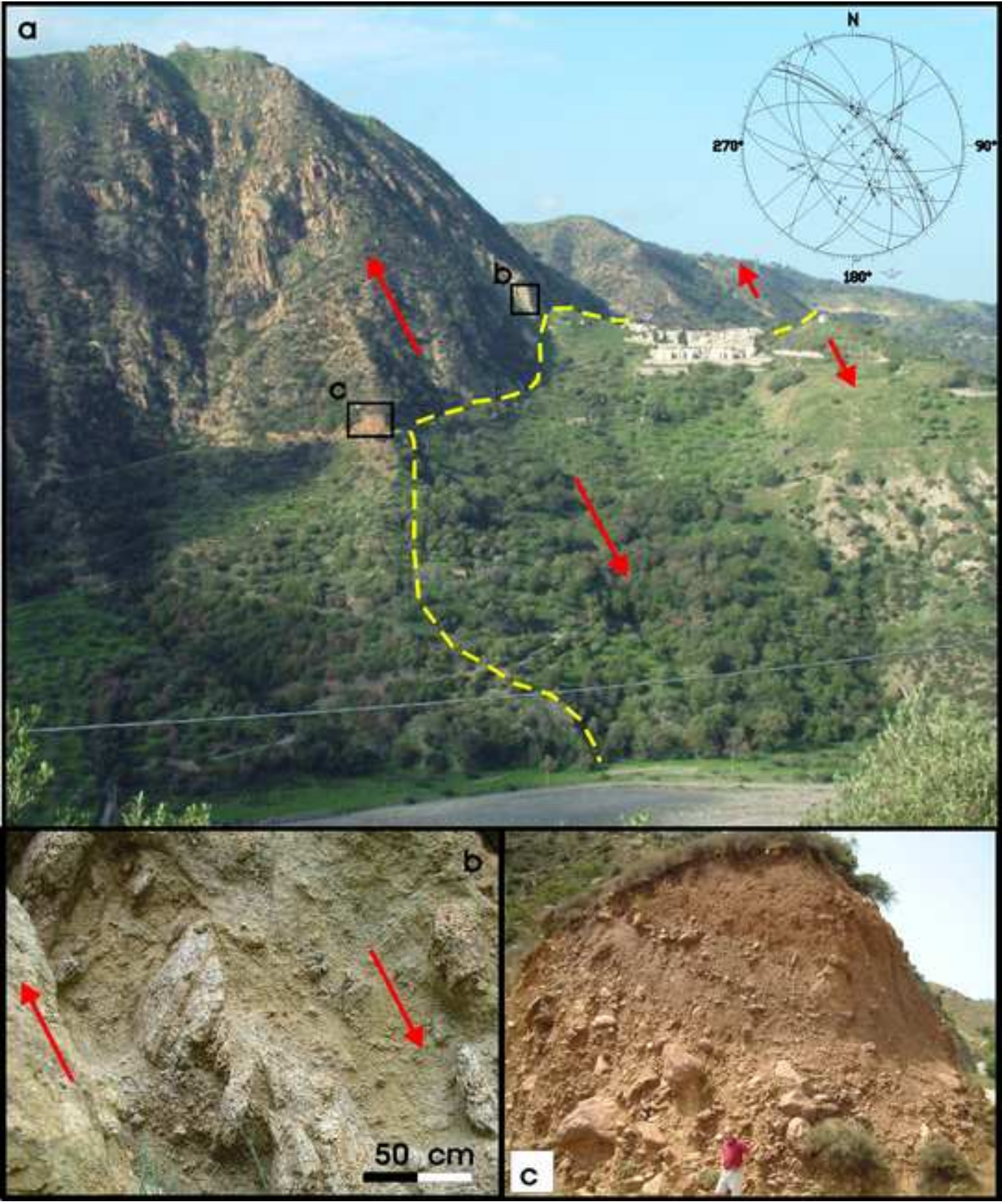
a
N
270°
90°
180°
b
c
b
50 cm
c


b
c
c
a
α
T. Tripi
T. Mazzarrà


d

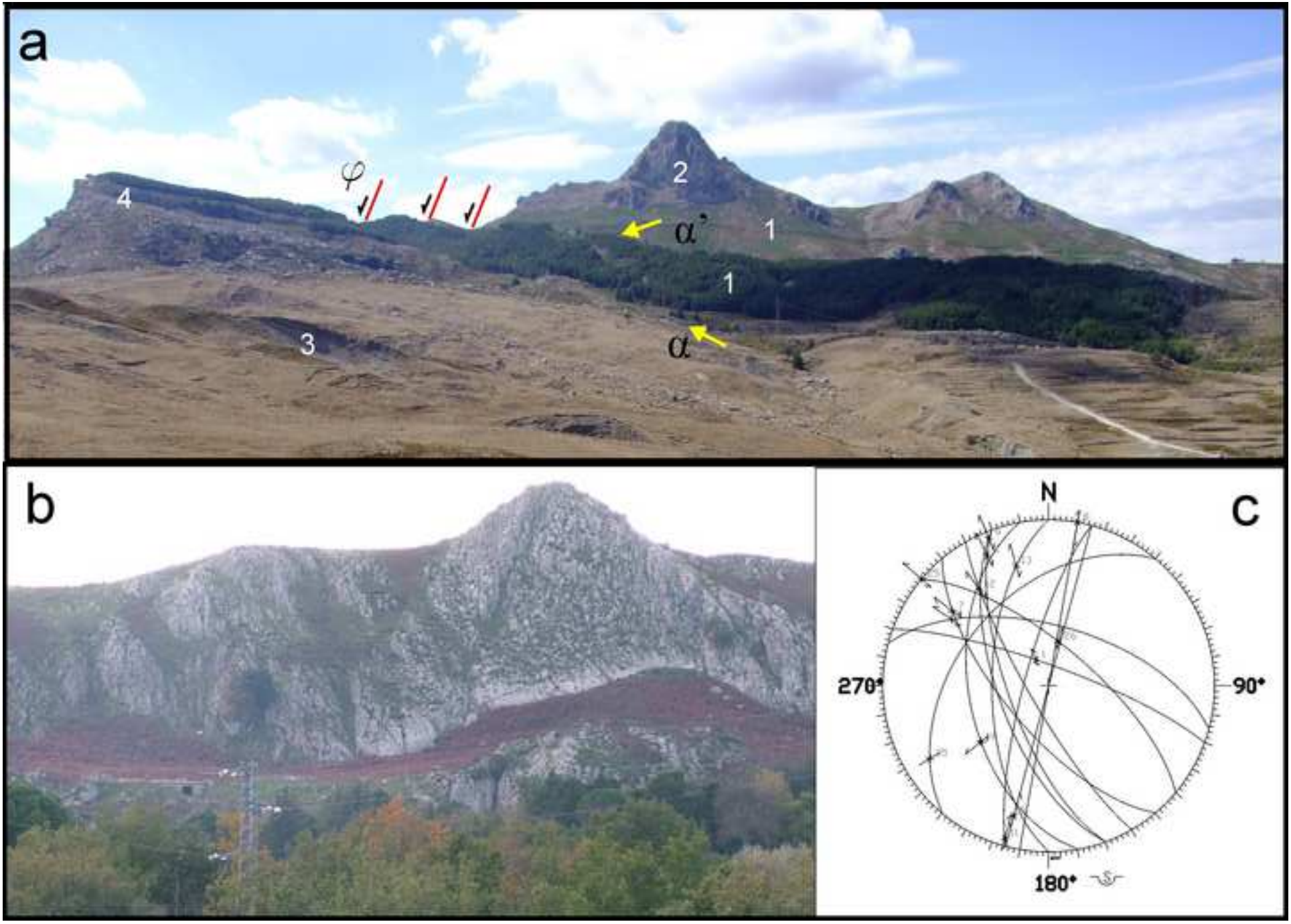
a
φ
2
4
α
1
1
3
α
b
N
c
270°
90°
180°
S

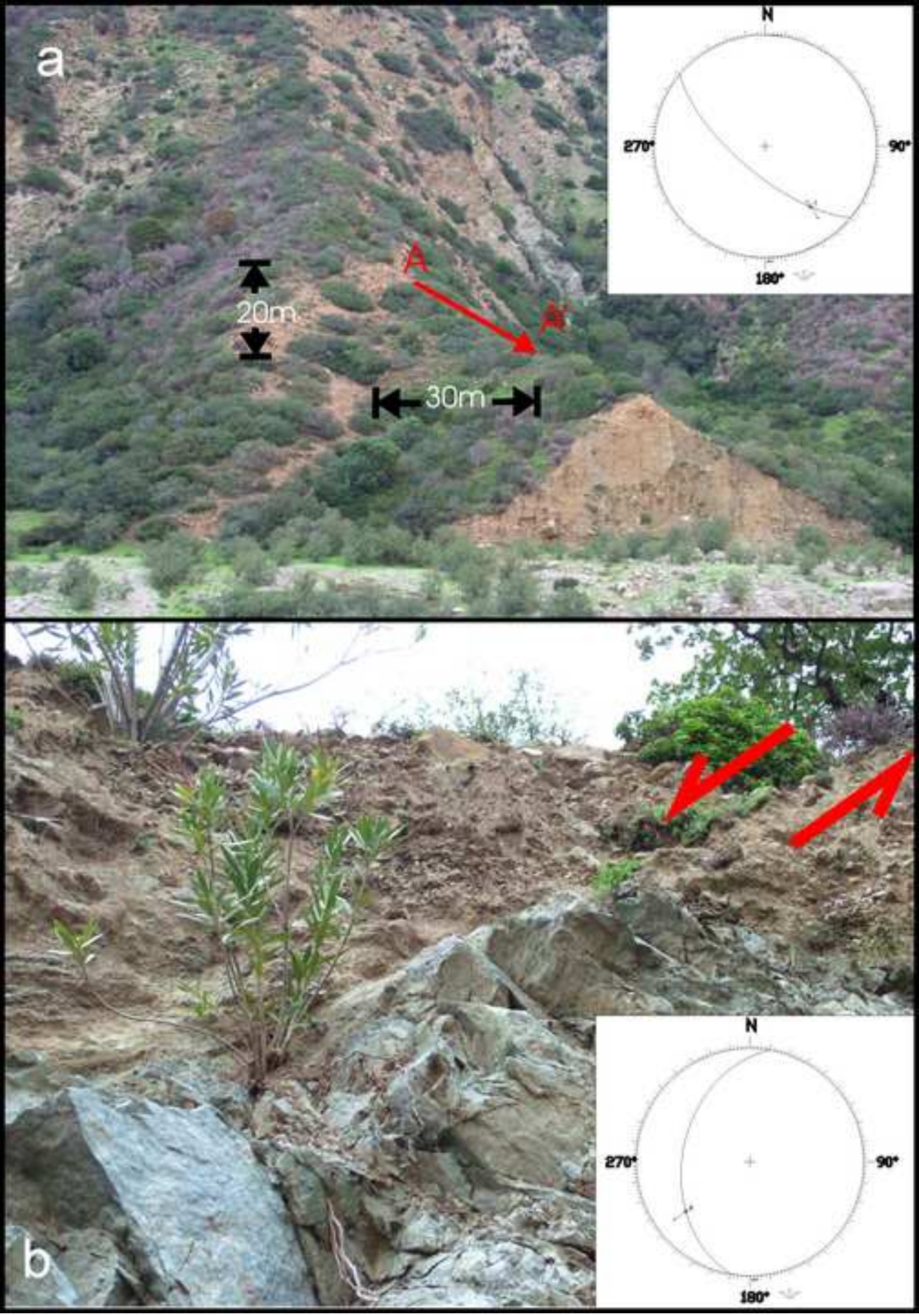
a
A
A'
20m
30m
N
270°
90°
180°
b
N
270°
90°
180°

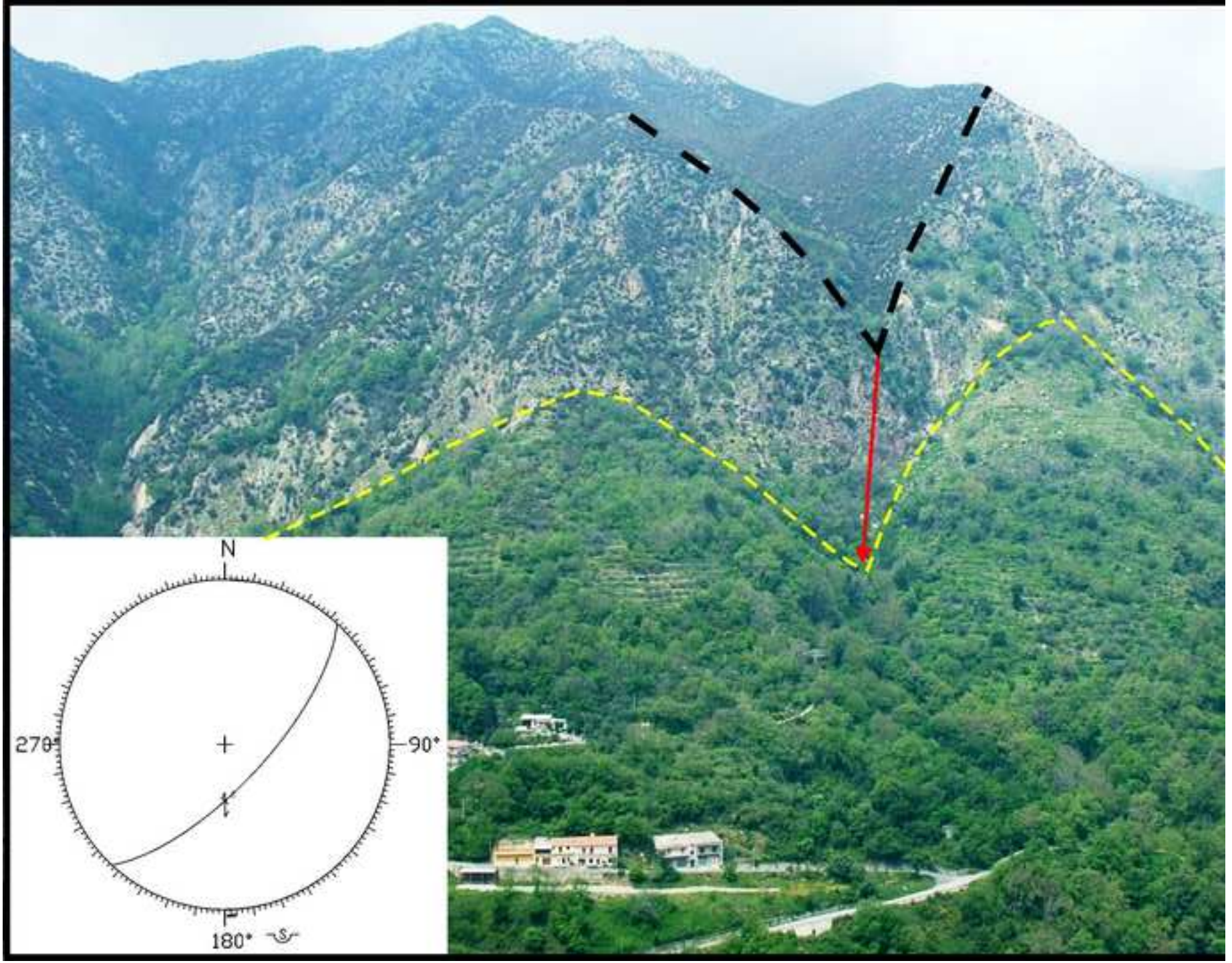
N
270°
90°
180°
S

Figure 12

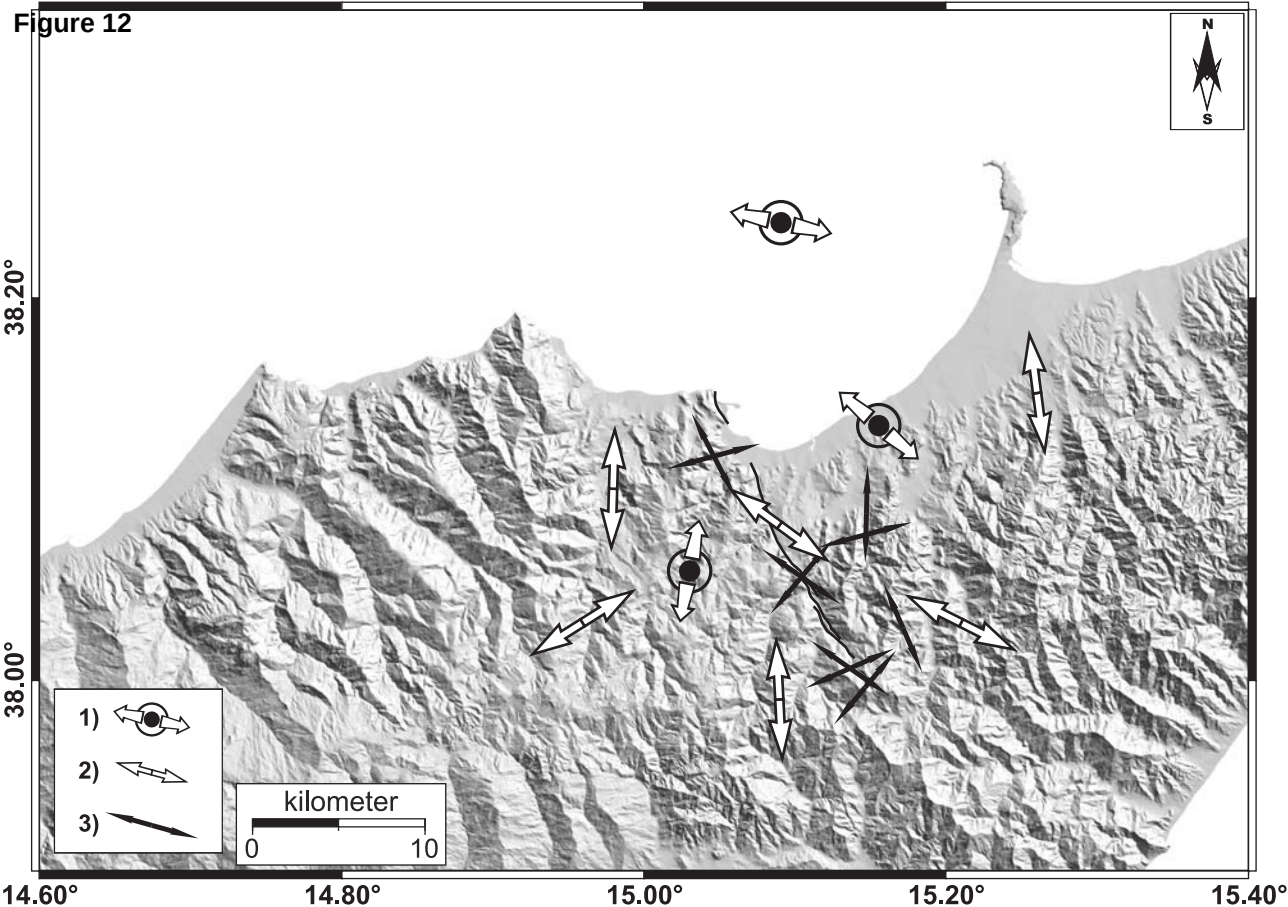

Table S1. Site code, geodetic coordinates, east and north velocity components referred to a fixed a fixed Eurasian frame (Mattia et al., 2008) frame for all GPS stations included in the processing. For each site, associated errors (95% of confidence), the correlation between the east and north components of velocity (RHO) and the observation history are also reported.

Site	Lon	Lat	V_E	V_N	s V_E	s V_N	RHO	V_U	s V_U	First obs.	Last obs.	N° obs.	Time span
	deg	*deg*	*mm/yr*	*mm/yr*	*mm/yr*	*mm/yr*		*mm/yr*	*mm/yr*				*years*
AJAC	8.763	41.927	-0.27	0.57	0.11	0.11	0.002	-0.09	0.23	2001.46	2008.25	1816	6.79
CAGL	8.973	39.136	0.96	0.78	0.10	0.10	0.035	2.21	0.12	1996.17	2008.25	4195	12.08
GRAS	6.921	43.755	-0.17	0.25	0.09	0.09	0.026	0.3	0.14	1996.00	2008.25	3995	12.25
GRAZ	15.493	47.067	0.4	0.2	0.09	0.09	-0.011	-0.94	0.13	1996.00	2008.25	4324	12.25
LAMP	12.606	35.5	-2.2	3.7	0.11	0.11	0.026	2.74	0.19	1999.23	2008.25	3103	9.02
MATE	16.704	40.649	1.51	4.64	0.09	0.09	-0.063	3.04	0.13	1996.00	2008.25	4432	12.25
MEDI	11.647	44.52	0.97	1.56	0.10	0.10	-0.004	-2.84	0.13	1996.17	2008.25	4235	12.08
NOT1	14.99	36.876	-0.82	5	0.11	0.11	0.005	3.47	0.21	2000.71	2008.25	2688	7.54
NOTO	14.99	36.876	-2.06	3.72	0.11	0.11	0.008	-1.19	0.57	1996.00	2000.73	1612	4.73
ZIMM	7.465	46.877	0.03	0.59	0.09	0.09	0.007	-0.41	0.12	1996.00	2008.25	4439	12.25
9518	15.005	37.951	-1.79	6.1	0.14	0.14	0.033	0.49	0.59	1996.52	2006.92	56	10.40
CALA	14.92	38.18	-1.12	7.28	0.23	0.24	-0.008	0.45	0.65	1998.90	2006.91	8	8.01
FDNV	14.919	38.1	-2.16	4.97	0.49	0.43	0.014	-7.7	1.69	2002.81	2006.92	12	4.11
FLOR	14.906	37.989	-3.94	3.73	0.52	0.44	0.009	-3.39	1.45	2002.81	2006.91	9	4.10
MAND	15.29	38.024	2.44	-0.55	0.48	0.39	-0.02	-5.86	1.49	1996.81	2002.82	7	6.01
MILA	15.231	38.271	0.38	4.58	0.35	0.34	0.008	2.02	0.73	2005.47	2008.33	904	2.86
MNGR	15.183	37.947	-3.15	3.64	0.57	0.47	0.001	0.54	1.69	2002.81	2006.91	7	4.10
MONT	15.014	38.024	-0.69	7.07	0.20	0.16	0.011	-2.81	0.53	1996.81	2007.44	73	10.63
NOVA	15.136	38.029	1.15	4.15	0.46	0.42	0.007	-2.21	1.34	2002.81	2006.93	20	4.12
RODI	15.167	38.108	0.75	4.92	0.51	0.43	0.01	-0.64	1.38	2002.81	2006.93	16	4.12
SPNC	15.353	38.146	-0.45	6.51	0.56	0.47	0.015	15.21	1.59	2002.81	2006.88	13	4.07
TIND	15.036	38.138	-2.06	7.35	0.26	0.20	-0.007	5.07	0.7	1998.90	2006.91	9	8.01

Table S2. Principal strain-rates and 1σ uncertainties computed for each quadrilateral reported in Fig. 3b. Positive and negative values represent extension and contraction respectively (φ is the azimuth of ε_{Hmax}).

Quadrilateral	Sites	Barycentre		$\varepsilon_{Hmax} \pm 1\sigma$ (nanostrain/yr)	$\varepsilon_{hmin} \pm 1\sigma$ (nanostrain/yr)	$\varphi \pm 1\sigma$ (deg)
		Long.	Lat.			
P1	MONT - CALA - TIND - FDNV	14.9775	38.1020	38.1 ± 60.7	-71.8 ± 45.0	1.3 ± 26.8
P2	MONT - FLOR - 9518 - FDNV	14.9600	38.0255	430.3 ± 141.8	-52.6 ± 4.0	57.9 ± 5.2
P3	NOVA - RODI - TIND - MONT	15.0905	38.0810	322.7 ± 9.9	-65.0 ± 96.9	125.5 ± 5.8
P4	NOVA - MNGR - 9518 - MONT	15.0941	37.9881	114.7 ± 74.9	15.4 ± 36.4	357.0 ± 22.2
P5	NOVA - MAND - MNGR - RODI	15.2130	38.0274	218.4 ± 50.9	2.5 ± 115.7	116.8 ± 25.3
P6	MILA - RODI - SPNC - MAND	15.2600	38.1475	159.1 ± 41.7	-44.2 ± 85.1	352.7 ± 19.5